This is a repository copy of *miR-132 suppresses transcription of ribosomal proteins to promote protective Th1 immunity*.

White Rose Research Online URL for this paper:
https://eprints.whiterose.ac.uk/143286/

Version: Accepted Version

Article:

1   **miR-132 suppresses transcription of ribosomal proteins to promote protective**

2   **Th1 immunity**

3

4   **James P. Hewitson[1], Kunal M. Shah[2], Najmeeyah Brown[1], Paul Grevitt[2], Sofia**

5   **Hain[1], Katherine Newling[3], Tyson V. Sharp[2], Paul M. Kaye[1], and Dimitris Lagos[1*]**

6

7   1. Centre for Immunology and Infection, Hull York Medical School and Department of

8   Biology, University of York, Wentworth Way, York, YO10 5DD, UK.

9   2. Centre of Molecular Oncology, Barts Cancer Institute, John Vane Science Centre,

10   Charterhouse Square, Queen Mary University London, London, EC1M 6BQ, UK.

11   3. Genomics and Bioinformatics Laboratory, Bioscience Technology Facility,

12   Department of Biology, University of York, Wentworth Way, York, YO10 5DD, UK.

13   * Corresponding author: dimitris.lagos@york.ac.uk, ORCID: 0000-0003-0637-281X.

14

17

18   **Short summary**

19   **The miR-132/212 cluster suppresses generation of IL-10-expressing Th1 cells**

20   **during chronic infection. This is associated with miR-132/212-mediated**

21   **suppression of ribosomal protein transcription in Th1 cells through silencing**

22   **BTAF1 and p300.**

23

24   **Highlights**

25   **- The transcriptomic hallmark of miR-132/212 deficiency in splenic CD4+ T cells**

26   **during chronic infection with *Leishmania donovani* is an up-regulation of several**

27   **ribosomal protein genes.**

28 **- The miR-132/212 cluster controls ribosomal protein expression through directly**

29 **targeting two transcriptional co-activators, BTAF1 and p300.**

30 **- *Leishmania donovani*-infected *miR-132/212$^{-/-}$* mice display increased IL-10 and**

31 **reduced IFNγ protein expression in Th1 cells, reduced hepatosplenomegaly, and**

32 **increased parasite burdens.**

33

34 **ABSTRACT**

35 **Determining the mechanisms that distinguish protective immunity from**

36 **pathological chronic inflammation remains a fundamental challenge. miR-132 has**

37 **been shown to play largely immunoregulatory roles in immunity, however its role**

38 **in CD4^{+} T cell function is poorly understood. Here, we show that CD4^{+} T cells**

39 **express high levels of miR-132 and that T cell activation leads to miR-132 up-**

40 **regulation. The transcriptomic hallmark of splenic CD4^{+} T cells lacking the miR-**

41 **132/212 cluster during chronic infection is an increase in mRNAs levels of**

42 **ribosomal protein (RP) genes. BTAF1, a co-factor of B-TFIID and novel miR-**

43 **132/212-3p target, and p300 contribute towards miR-132/212-mediated regulation**

44 **of RP transcription. Following infection with *Leishmania donovani miR-132$^{-/-}$* CD4^{+}**

45 **T cells display enhanced expression of IL-10 and decreased IFNγ. This is**

46 **associated with reduced hepatosplenomegaly and enhanced pathogen load. The**

47 **enhanced IL-10 expression in *miR-132$^{-/-}$* Th1 cells is recapitulated *in vitro***

48 **following treatment with phenylephrine, a drug reported to promote ribosome**

49 **synthesis. Our results uncover that miR-132/212-mediated regulation of RP**

50 **expression is critical for optimal CD4^{+} T cell activation and protective immunity**

51 **against pathogens.**

52

53 **INTRODUCTION**

54 MicroRNAs (miRNAs) are endogenous small silencing RNAs with fundamental roles in

55 the immune system [1]. In this context, miR-132-3p (miR-132) is derived from the miR-

56 212/132 cluster and has emerged as key regulator of immune cell development and

57 function [1, 2]. During innate immune activation, miR-132 is induced upon and plays a

58 crucial role in the transcriptional response to pathogenic challenge [3-6]. We have

59 previously shown that miR-132 is induced in a dose-dependent manner upon viral

60 infection and suppresses the innate antiviral immune response by down-regulating

61 expression of p300 (official symbol EP300), a necessary co-activator for several key

62 transcription factors [3]. Furthermore, miR-132 has been shown to be critical for normal

63 haematopoiesis and B cell development and function through suppression of FOXO3

64 and SOX4, respectively [7, 8], whereas the miR-212/132 cluster has also been

65 implicated in Th17 responses [9]. miR-132 is also up-regulated in a model of

66 inflammation-induced cellular transformation [10], plays a key role inflammation during

67 wound healing [11], is induced *in vivo* following infection by *Toxoplasma gondii* [12], and

68 regulates macrophage activation following *Mycobacterium tuberculosis* infection [13].

69 Although the above studies have provided strong support for the role of miR-132 in the

70 immune system, they have predominantly focused on acute inflammation or infection

71 models whereas the role of miR-132 in models of pathogen-induced chronic

72 inflammation remains poorly explored. For example, we have limited knowledge on

73 whether miR-132 is dispensable for T cell-mediated immunity.

74

75 Here we show that miR-132 is induced upon activation of CD4$^+$ T cells *in vitro* and *in*

76 *vivo* during infection of mice with *Leishmania donovani* (*L. donovani*). Using fully *miR-*

77 *212/132*-deficient mice [14] (hereafter referred to as *miR-132$^{-/-}$* mice), we show that the

78 transcriptomic hallmark of miR-132 deficiency in CD4$^+$ T cells isolated from chronically

79 infected spleens is an increase in mRNAs levels of ribosomal protein (RP) genes.

80 Similarly, miR-132 controls RP gene mRNA levels during *in vitro* activation of CD4$^+$ T

81 cells. Enhanced ribosome biosynthesis during *in vitro* CD4$^+$ T cell activation is thought

82 to be necessary for accommodating the needs for cytokine production in activated cells

83 [15]. However, the *in vivo* relevance of this phenomenon and the molecular drivers

84 underpinning it remain largely unexplored. Notably, miR-132 over-expression

85 suppresses RP gene expression and protein synthesis rates in mouse embryonic

86 fibroblasts (MEFs). Regulation of RP gene expression is mediated by miR-132-mediated

87 silencing of proteins involved in transcription including p300 and BTAF1, which we

88 identified here as a novel miR-132 target. *In vivo*, *miR-132*^{-/-} CD4^{+} T cells from

89 chronically infected mice express higher levels of IL-10 and lower levels of IFNγ when

90 compared to WT cells. This functional impairment correlates with reduced

91 immunopathology and increased pathogen burdens in *L. donovani*-infected miR-132^{-/-}

92 mice. *In vitro*, activated *miR-132*^{-/-} CD4^{+} T cells treated with the hypertrophic factor

93 phenylephrine (PE) also demonstrate enhanced IL-10 expression. Overall, the above

94 demonstrate that miR-132 is a necessary and sufficient regulator of RP gene expression

95 through targeting core transcriptional regulators and that this mechanism contributes

96 towards optimal CD4^{+} T cell activation and protective immunity.

97

98 **RESULTS AND DISCUSSION**

99 **miR-132 is up-regulated during CD4^{+} T cell activation**

100 We first determined whether miR-212/132 levels were regulated following stimulation of

101 naïve (CD62L^{+} CD44^{-}) CD4 T cells with anti-CD3 and anti-CD28 antibodies, and found

102 strong miR-132-3p and -212-3p up-regulation that peaked at day 1 (18hrs) (**Fig. 1A**; ~20

103 and ~30 fold increase compared to unstimulated cells) and remained elevated for at

104 least 3 days. Expression of the *miR-212/132* primary transcript is CREB-dependent [16],

105 and as expected [17], TCR stimulation induced strong CREB phosphorylation within 2-

106 4 hours, and this was sustained for 3 days (**Fig. EV1A**). Whilst miR-146-5p showed little

107 change following T cell activation, miR-155-5p was strongly up-regulated for sustained

108 periods, whereas miR-16-5p levels declined (**Fig. 1A**). miR-132-3p and miR-212-3p up-

4

109 regulation appeared to be a common feature in activated CD4$^+$ T cells, and occurred

110 regardless of T cell polarisation phenotype (Th0, Th1 and Th2; **Fig. EV1B**).

111 To investigate the role of miR-212/132 in the development of inflammation and

112 protective immune responses *in vivo*, we studied its expression in naïve and infected

113 C57BL/6 WT mice with *L. donovani* amastigotes. This infection model allows the study

114 of host-pathogen interactions [18], during which infection occurs in the liver, spleen, and

115 bone marrow. We sorted splenic lymphocytes and found that CD4$^+$ T cells express

116 higher miR-132-3p levels than CD8$^+$ T cells or B cells (**Fig. 1B**). Furthermore, *L.*

117 *donovani* infection resulted in miR-132-3p up-regulation in CD4$^+$ T cells. The extent of

118 this up-regulation was similar to that observed for miRNAs previously reported to be

119 involved in T cell responses such as 146-5p and 155-5p [19, 20]. Combining these

120 results with previous findings demonstrating miR-132 induction downstream of TLR [3-

121 5] and the B cell receptor [7] establishes miR-132 induction as a hallmark of innate and

122 adaptive immune activation. Of note, miR-132 up-regulation has also been observed in

123 studies using human bulk CD4$^+$ and CD8$^+$ T cell populations where it was amongst the

124 most prominent up-regulated miRNAs [21].

125

126 **miR-212/132-deficiency is associated with global up-regulation of ribosomal**

127 **protein genes in CD4$^+$ T cells from chronically infected spleens.**

128 To gain a molecular understanding of the function of the miR-132/212 cluster in CD4$^+$ T

129 cells *in vivo*, we performed RNAseq analysis on biological replicates of sorted splenic

130 CD4$^+$ T cells from *L. donovani*-infected WT and *miR-132$^{-/-}$* mice. Of the more than 14,000

131 genes that were detectable in CD4$^+$ T cells, similar numbers showed up- or down-

132 regulation by >50% in *miR-132$^{-/-}$* compared to WT cells (**Fig. 1C**; 10.3% up and 10.6%

133 down). However, of the 1290 significantly differently expressed genes (9% of total),

134 approximately 2/3 (850) were up-regulated in *miR-132$^{-/-}$* cells compared to WT and only

135 1/3 (440) down-regulated. Pathway analysis of genes significantly up-regulated in *miR-*

136 *132$^{-/-}$* mice (p<0.05, >50% regulation) using the Gene Set Enrichment Analysis [22] and

137 STRING tools [23] revealed that a cluster of RP genes was significantly over-

138 represented amongst genes upregulated in *miR-132^(-/-)* CD4^+ T cells (**Fig. 1D and 1E**).

139 This up-regulation was evident for both small (RPS) and large (RPL) subunits protein

140 genes and even pseudogene transcripts (**Fig. 1F**). These results were further validated

141 by qPCR, showing an increase in all tested RP genes, reaching statistical significance

142 for RPL27, RPS10 and RPL14-ps1 (**Fig. 1G**). To explore the significance of the

143 observed increase in RP gene expression in *miR-132^(-/-)* CD4^+ T cells, we analysed

144 published transcriptional profiles of *in vitro* generated Th1 and Th2 cells [24] and found

145 that CD4^+ T cell activation results in a statistically significant shift towards global up-

146 regulation of RP gene levels (**Fig. 1H** and **Fig. EV1C**). Taken together with previous

147 reports demonstrating that activation of ribosome biosynthesis is associated with

148 activation of CD8^+ T cells [25] and production of cytokines by CD4^+ T cells *in vitro* [15],

149 our findings suggested that the observed RP gene up-regulation in *miR-132^(-/-)* CD4^+ T

150 cells was a signature of enhanced activation.

151

152 **The B-TFIID cofactor BTAF1 is a direct miR-132 target in CD4^+ T cells.**

153 To identify direct targets of the miR-132/212 cluster in CD4^+ T cells, we performed

154 RNAseq analysis of naïve CD4^+ T cells from WT and *miR-132^(-/-)* mice prior to and

155 following 1 day (18 hours) of *in vitro* TCR stimulation under Th1 conditions. We focussed

156 on Th1 responses as these predominate in *L. donovani* infection and these cells

157 displayed the highest levels of miR-132 expression (**Fig. EV1B)**. Broadly similar

158 numbers of transcripts were detected in unstimulated and stimulated T cells (12336 and

159 11140, respectively), with 5.0% (day 0 = 615) and 3.9% (day 1 = 432) showing significant

160 differences between WT and *miR-132^(-/-)* mice (**Fig. 2A-B**). A much larger number of

161 genes (44% WT, 54% *miR-132^(-/-)*) were differentially expressed when we compared

162 naïve with activated T cells (**Fig. EV2A-B**). Of the genes that were significantly different

163 between WT and *miR-132^(-/-)* mice (p<0.05; 50% difference), 46% were up-regulated in

164 *miR-132^(-/-)* at day 0, and this increased to 68% at day 1. At day 1, we observed that the

165 majority of predicted miR-132/212-3p targets were up-regulated (i.e. 51/75 =68%

166 displayed a positive log2 fold change) in *miR-132^-/-* CD4^+ T cells (**Fig. 2C-D**). Of note, a

167 single predicted miR-132/212-3p target, BTAF1, was up-regulated in both unstimulated

168 and activated *miR-132^-/-* CD4^+ T cells, as well as in CD4^+ T cells from *L. donovani-*

169 infected *miR-132^-/-* mice (**Fig. 2C-E, and Fig. EV2C**). Up-regulation of BTAF1 was

170 confirmed by qPCR (**Fig. 2F**). BTAF1 protein expression was elevated in *miR-132^-/-*

171 CD4^+ T cells compared to WT cells, both before and after TCR stimulation (**Fig. 2G**).

172 BTAF1 contains a single 7mer-m8 site for miR-132/212-3p within its 3'UTR that is

173 broadly conserved in mammals (**Fig. EV2D**). To assess whether BTAF1 was a direct

174 target of miR-132/212-3p, we transfected HeLa or 3T3 cells with luciferase reporter

175 constructs preceded by ~1.5kb of *BTAF1* 3'UTR (either WT or with miR-132/212-3p site

176 mutated) in the presence of miR-132-3p or miR-212-3p mimics. This revealed that in the

177 presence of miR-132-3p mimics, luciferase activity was significantly elevated following

178 mutation of the miR-132/212 site in the 3'UTR (**Fig. 2H, Fig. EV2E**). A similar trend was

179 observed in miR-212-3p transfected cells although this did not reach statistical

180 significance. This demonstrated that miR-132 can directly interact with the predicted

181 miR-132-binding site in the *BTAF1* 3' UTR. We also searched for potential miR-132-5p

182 and miR-212-5p targets that were altered in miR-132^-/- mice. Unlike miR-132-3p and

183 miR-212-3p, these two miRNA differ in their seed sequence and so are predicted to

184 have different mRNA targets (**Fig. EV2F**). Whilst several potential targets were

185 significantly dysregulated in miR-132^-/- CD4^+ cells, there was little overlap between those

186 altered in unstimulated T cells, d1 activated T cells or those derived from d28 *L.*

187 *donovani*-infection (**Fig. EV2G**). Only a single target, BACH2 (predicted 7mer-A1 target

188 for both miR-212-5p and miR-132-5p), was up-regulated by >50% in all three T cell

189 datasets, but this was only significant for *in vitro* d1 stimulated T cells and was highly

190 variable in the other two conditions (**Fig. EV2H**).

191 Having observed an effect of miR-132 deletion on RP gene mRNA levels after chronic

192 CD4^+ T cell activation *in vivo* (**Fig. 1**), we tested whether we can observe a similar effect

193   in our dataset from the early stages of *in vitro* CD4$^+$ T cell activation. Following 24h of *in*

194   *vitro* activation of naïve CD4$^+$ T cells, we observed that 40% of RP genes showed

195   upregulation (positive log$_2$ fold change or LFC) in *WT* mice. This proportion was

196   significantly increased to 61% in *miR-132$^{-/-}$* mice (P = 0.011) (**Fig. EV2I**). Furthermore,

197   the vast majority of RP genes (81%) demonstrated a higher LFC (indicating stronger up-

198   regulation or weaker downregulation) upon activation of *miR-132$^{-/-}$* CD4$^+$ T cells

199   compared to WT cells (**Fig. EV2J**).

200

201   **p300 and BTAF1 contribute to miR-132-mediated suppression of ribosomal**

202   **protein expression**

203   miR-132 deficiency resulted in upregulation of several RP genes in CD4$^+$ T cells from

204   chronically infected mice with *L. donovani* (**Fig. 1**). In addition, we found that miR-132-

205   3p or miR-212-3p over-expression in mouse embryonic fibroblasts (MEFs) resulted in

206   widespread down-regulation of RP gene mRNA levels (**Fig. 3A and EV3A**). These

207   effects were confirmed at the protein level using Rpl27 and Rps10 as two representative

208   RPs (**Fig. EV3B**). This allowed us to further probe the mechanism employed by miR-

209   132 to regulate ribosomal protein gene levels. The majority of RP transcripts up-

210   regulated in *miR-132$^{-/-}$* mice (**Fig. 1D**) lacked miR-132/212-3p sites (13/15 coding

211   transcripts), with the remaining 2/15 (RPL7L1 and RPL18) displaying non-conserved

212   sites. Predicted miR-132/212-3p targets are statistically significantly enriched in proteins

213   involved in transcription (**Fig. EV3C**). Therefore, we reasoned that the effect of miR-132

214   on RP gene expression was caused by miR-132-mediated suppression of transcriptional

215   regulators. For example, p300, a previously validated miR-132 target [3], is required for

216   the activity of Sp1, YY1 and CREB, all of which have known roles in transcription of RP

217   genes [26-28]. Of note, although miR-132 directly suppresses p300, its effects on p300

218   mRNA steady-state levels are minimal [3]. In parallel, BTAF1, a predominant miR-132

219   target in CD4$^+$ T cells (**Fig. 2**) interacts with TATA-binding protein (TBP) to form B-TFIID,

220   causing redistribution of TBP to new genomic sites [29, 30]. Over-expression of miR-

221 132 in MEFs resulted in suppression of p300 and BTAF1 (**Fig. 3B**). Similarly, over-

222 expression of miR-132-3p or miR-212-3p in the EL4 T cell line also resulted in

223 suppression of BTAF1 and p300 (**Fig. EV3D**) suggesting that both miRNAs contribute

224 to regulation of BTAF1 and p300. Knockdown of p300 resulted in significant

225 downregulation of several miR-132-regulated RP transcript levels, including RPL27,

226 RPSA, RPS3A, RPS9, RPS10, and RPL14-ps1 (**Fig. 3C**), whereas levels of RPL18

227 showed a trend towards downregulation (P=0.06). In addition, knockdown of BTAF1

228 significantly reduced levels of RPL27 and RPL18, with RPL14-ps1 showing a trend

229 towards downregulation (P=0.052) (**Fig. 3D**). Critically, suppression of RP expression

230 by miR-132 was dependent on both p300 and BTAF1 (**Fig. 3E**). Although the majority

231 of miR-132-mediated effects on RP expression were abolished upon knockdown of

232 either p300 or BTAF1, we also identified RP mRNAs that were specifically dependent

233 on p300 (e.g. miR-132-mediated suppression of Rps9) or BTAF1 (e.g. miR-132-

234 mediated suppression of Rpl18; **Fig. 3E**). To validate the functional relevance of these

235 effects we tested protein synthesis rates in MEFs over-expressing miR-132-3p or miR-

236 212-3p using a puromycin incorporation assay [31]. Over-expression of either of the two

237 miRNAs resulted in suppression of protein synthesis, consistent with their effect on RP

238 expression (**Fig. 3F**). These findings demonstrate that p300 and BTAF1, two miR-132

239 targets involved in transcription, contribute towards the widespread regulation of RP

240 genes observed in miR-132/212-deficient or over-expressing cells. Interestingly, Mot1,

241 the yeast homologue of BTAF1, promotes expression of ribosomal proteins in yeast [32],

242 as seen here for BTAF1 and RPL27 and RPL18 in mouse cells. We should note that

243 given the number of potential miR-132 targets involved in transcription (**Fig. EV3C**)[33],

244 we cannot exclude the contribution of additional miR-132 targets towards RP gene

245 regulation. Importantly, it is thought that the majority of RP genes are not regulated at

246 the post-transcriptional level by miRNAs due their relatively short 3'UTRs [34]. However,

247 our work demonstrates that a miRNA can indirectly suppress a cluster of RP genes in

248 CD4$^+$ T cells and MEFs. This reveals a novel mechanism of RP regulation with miR-132

249 acting as a molecular node mediating crosstalk between RP expression and post-

250 transcriptional gene silencing.

251

252 **The miR-212/132 cluster controls the balance between IL-10 and IFNγ production**

253 **in CD4$^+$ T cells.**

254 Having shown that miR-132 deficiency results in similar transcriptomic effects in CD4$^+$

255 cells *in vitro* and *in vivo* (e.g. RP gene regulation, BTAF1 suppression) and during *L.*

256 *donovani* infection (**Figs. 1 and 2**), we measured capacity for IFNγ and IL-10 production

257 by CD4$^+$ T cells from infected mice by intracellular cytokine staining following *ex vivo*

258 stimulation with PMA and ionomycin. We found a modest but significant reduction in the

259 ability of *miR-132$^{-/-}$* CD4$^+$ T cells to produce IFNγ (**Fig. 4A**). This was accompanied by

260 a greater fold increase in production of IL-10 by *miR-132$^{-/-}$* IFNγ$^+$ CD4$^+$ T cells compared

261 to wild-type cells (**Fig. 4B and Fig. EV4A**). Interestingly, IL-10 mRNA levels were not

262 statistically significantly different between *WT* and *miR-132$^{-/-}$* cells (**Fig. 4C**), indicating

263 that miR-132 affected IL-10 expression at the post-transcriptional/translational level.

264 Increased IL-10 production by miR-132$^{-/-}$ CD4$^+$ T cells was also evident following *in vitro*

265 restimulation of splenic CD4$^+$ T cells from infected mice with *L. donovani* antigen

266 demonstrating that the effect was occurring in antigen-specific manner (**Fig. EV4B**). The

267 observed reduction in frequency of IFNγ$^+$ CD4$^+$ T cells and an increase in frequency of

268 IFNγ$^+$IL-10$^+$ CD4$^+$ T cells is consistent with the concept that IL-10$^+$ Th1 cells develop

269 after prolonged exposure to antigen and represent an endpoint of the Th1 response [35].

270 In this respect, our results can be interpreted as *miR-132$^{-/-}$* CD4$^+$ T cells reaching this

271 endpoint immunoregulatory status prematurely.

272 At the molecular level, the increase in IFNγ$^+$IL-10$^+$ CD4$^+$ T cells *in vivo* was associated

273 with a transcriptomic signature characterised by an up-regulation of a cluster of RP

274 genes in *miR-132$^{-/-}$* CD4$^+$ T cells (**Fig. 1D-E**). To further explore this finding we compared

275 *in vitro* Th1 differentiation of WT and *miR-132$^{-/-}$* CD4$^+$ T cells in presence or absence of

276 phenylephrine (PE), which has been shown to enhance ribosome biosynthesis [36].

277 Remarkably, although there were no statistically significant differences between *miR-*

278 *132^-/-* and WT cells, nor between WT DMSO-treated and PE-treated cells, treating *miR-*

279 *132^-/-* CD4^+ T cells with PE resulted in statistically significantly enhanced IL-10

280 expression and increased number of cells compared to WT cells. An increase in IL-10

281 levels was observed in PE-treated WT cells compared to DMSO-treated WT cells but

282 this did not reach statistical significance. IFNγ levels were not affected by PE and were

283 lower in *miR-132^-/-* Th1 cells although this did not reach significance after multiple testing

284 correction (**Fig. 4D-F**). In agreement with our *in vivo* observations, the enhanced cell

285 number and IL-10 expression under these *in vitro* conditions recapitulated enhanced

286 activation and premature acquisition of an immunoregulatory state in *miR132^-/-* CD4^+ T

287 cells. Overall, these results demonstrated that miR-132 connects RP expression, IL-10

288 expression, and CD4^+ T cell activation in Th1 cells. Our results infer that the observed

289 deregulation of selected RPs in *miR-132^-/-* CD4^+ T cells *in vivo* likely alters the

290 composition and function of ribosomes in a manner that specifically promotes IL-10

291 expression. This could be potentially explained by formation of specialised ribosomes in

292 activated CD4^+ T cells [37, 38].

293

294 **The miR-212/132 cluster promotes protective immunity to *L. donovani*.**

295 Having observed that loss of miR-132 favours an immunoregulatory (higher IL-10

296 expression) phenotype in Th1 cells, we tested the response of miR-132^-/- mice to *L.*

297 *donovani* infection. Indeed, IFNγ^+IL-10^+ CD4^+ T cells have been associated with immune

298 dysregulation and infection susceptibility in a variety of human and experimental

299 systems [39-43]. Furthermore, the role of IL-10 in preventing *L. donovani* clearance had

300 been previously demonstrated [44-46]. However this support comes from the study of

301 fully IL-10-deficient mice and use of blocking antibodies against IL-10 or its receptor. To

302 determine whether modest changes in IL-10 levels could alter infection outcomes, we

303 infected *IL-10^+/+*, *IL-10^+/-* and *IL-10^-/-* mice. Infected *IL-10^+/-* mice produced intermediate

304 levels of IL-10 compared to their *IL-10^+/+* and *IL-10^-/-* counterparts (**Fig. EV5A**), without

305 any change in IFNγ production (**Fig. EV5B**). Notably, as with WT mice treated with IL-

306 10R-blocking antibody or *IL-10^{-/-}* mice, *IL-10^{+/-}* mice were able to clear liver parasites

307 albeit with slower kinetics (**Fig. 5A**). These experiments suggested that modifying the

308 relative abundance of IL-10 and IFNγ by reducing IL-10 by 50% can affect susceptibility

309 to *L. donovani* infection. Consistently with these findings and the observed IL-10 levels

310 in *miR-132^{-/-}* mice, *L. donovani* infection resulted in significantly elevated splenic

311 parasite burdens in *miR-132^{-/-}* mice (**Fig. 5B**). Although we observed variation in parasite

312 load between different experiments (**Fig. 5C**), *miR-132^{-/-}* spleens consistently harboured

313 approximately 2-fold more parasites at day 28 compared to WT controls (**Fig. 5C-D**). In

314 addition to parasite loads miR-132 deficiency affected CD11b^{+} cell populations, here

315 called MφA (CD11b^{+} F4/80^{+} CD11c^{-}), MφB (CD11b^{hi} F4/80^{hi} CD11c^{+}), and MφC

316 (CD11b^{hi} F4/80^{lo} CD11c^{+}) present in infected spleens (gated as **Fig. EV5C**). The

317 numbers of MφA and MφB cells decreased in infected *miR-132^{-/-}* mice characterised by

318 higher IL-10 expression in CD4^{+} T cells (**Fig. EV5D**). Conversely, numbers of these

319 populations increased in an IL-10 dose dependent manner, in infected *IL-10^{-/-}* and to a

320 lesser extent in *IL-10^{+/-}* mice (**Fig. EV5E**), demonstrating that the number of these cells

321 is inversely correlated with IL-10 expression. Of note, IL-10 expression did not differ

322 between *WT* and *miR-132^{-/-}* myeloid subpopulations (**Fig. EV5F**). This demonstrated

323 that the effect of miR-132 on IL-10 expression does not occur in all IL-10-producing cell

324 types, showing specificity for Th1 cells. Our findings do not exclude that miR-132-

325 mediated suppression of IL-10 might occur in other cell types (e.g. B cells, innate

326 lymphoid cells) contributing to the overall function of miR-132 in immunity.

327 Liver parasite burdens peaked around day 21 and we noted increased levels in *miR-*

328 *132^{-/-}* mice at this time point (**Fig. EV5G**). Whilst *miR-132^{-/-}* liver burdens were only

329 significantly elevated at day 28 when we corrected for inter-experiment variations in

330 infection intensity (**Fig. EV5H**), *miR-132^{-/-}* mice continued to harbour a significantly

331 elevated parasite burden at day 42 (**Fig. EV5I**), a time point when parasites are being

332 cleared from this organ in WT C57BL/6 mice [18]. Notably, the enhanced pathogen

333 burdens coincided with significantly smaller spleen and liver size in *miR-132$^{-/-}$* mice

334 compared to their WT counterparts (**Fig. 5E-F**). The impact of miR-132 deficiency on

335 hepatosplenomegaly was most pronounced at higher infection levels, with a similar

336 trend also evident after infection with lower parasite doses (**Fig. EV5J-K**).

337 In sum, we propose that our findings support a model according to which enhanced

338 ribosomal protein expression upon activation of miR-132$^{-/-}$ CD4^{+} T cells *in vivo*

339 contributes towards accelerated activation of these cells and the premature switch to

340 the IFNγ^{+}IL-10^{+} phenotype. Although we cannot exclude that other cell types or

341 mechanisms contribute to the observed increase in parasite loads in *miR-132$^{-/-}$* mice,

342 we propose that the effects of miR-132 deficiency on IL-10 expression in IFNγ^{+} CD4^{+} T

343 cells significantly contribute to reduced protective inflammation and enhanced

344 susceptibility of *miR-132$^{-/-}$* mice to infection. This is consistent with previous publications

345 that highlight that IL-10 produced by Th1 cells (rather than regulatory T cells or myeloid

346 cells) is a critical determinant of *L. donovani* infection outcomes [40, 47]. Of note, due

347 to the impossibility of concurrent physiological knockdown or over-expression of RPs,

348 the functional relevance of this family of proteins to Th1 responses *in vivo* has remained

349 elusive. Our results provide a novel conceptual framework for the *in vivo* relevance of

350 RP expression in CD4^{+} T cells indicating that exaggerated RP expression can be

351 associated with impaired T cell responses. We propose that miR-132-driven

352 coordination of the machineries that control RNA metabolism is essential for optimal Th1

353 cell activation and protective immunity.

354

355 **MATERIALS AND METHODS**

356 **Ethics**

357 Animal care and experimental procedures were regulated under the Animals (Scientific

358 Procedures) Act 1986 (revised under European Directive 2010/63/EU) and were

359 performed under UK Home Office License (project licence number PPL 60/4377 with

360 approval from the University of York Animal Welfare and Ethical Review Body). Animal

361 experiments conformed to ARRIVE guidelines.

362

363 **Mice and *L. donovani* infection**

364 Female C57BL/6 CD45.1, CD45.2, and RAG2^{-/-} mice were obtained from Charles River

365 (UK). *MiR-132/212[-/-]* mice (complete knockouts) were provided by Dr Richard Goodman

366 (Vollum Institute, Oregon Health & Science University, USA). IL-10^{-/-} mice were provided

367 by Dr Anne O'Garra (Francis Crick Institute, UK) and were crossed with WT CD45.2

368 C57BL/6 mice to generate IL-10^{+/-} heterozygotes. All mice were bred in house,

369 maintained under specific pathogen-free conditions and used at 6 – 12 weeks of age.

370 The Ethiopian strain of *L. donovani* (LV9) was maintained by passage in RAG-2^{-/-} mice.

371 Mice were infected i.v. with 100×10^6 amastigotes via the tail vein. Parasite doses of 10

372 and 30×10^6 were also used where indicated. Parasite burden was expressed as

373 Leishman-Donovan units (LDU; the number of parasites per 1,000 host cell nuclei ×

374 organ weight in mg)[48]. To allow comparison between these experiments, we

375 normalised LDU to the levels observed in WT mice (relative LDU). For IL-10R

376 neutralisation experiments mice were infected with *L. donovani* and received anti-IL10R

377 (Clone: 1B1.3A from Bio X Cell) or IgG isotype control (SIGMA) injections at day 0, 14,

378 and 21 p.i. at 0.5mg mAb/injection.

379

380 **FACS analysis and cell sorting.**

381 For FACS analysis, spleens were first digested with 0.4 U/ml Liberase TL (Roche) and

382 80 U/ml DNase I type IV in Hank's Balanced Salt Solution (both Sigma) for 15min at

383 37°C. Enzyme activity was inhibited with 10mM EDTA pH 7.5 and single cell

384 suspensions created with 70 µm nylon filters (BD Biosciences) in complete RPMI 1640

385 (ThermoFisher) supplemented with 10% heat inactivated FCS (HyClone), 100 U/ml

386 penicillin, 100 µg/ml streptomycin and 2 mM L-glutamine (all ThermoFisher). Red blood

387 cells were lysed with red blood cell lysing buffer (Sigma), For live/dead discrimination,

388 cells were washed twice in PBS, then stained with Zombie Aqua (Biolegend) before

389 resuspension in FACS buffer (PBS containing 0.5% BSA and 0.05% azide). Fc

390 receptors were blocked with 100µg/ml rat IgG (Sigma) for 10min at 4°C, before surface

391 staining for 30min at 4°C. Combinations of the following anti-mouse antibodies were

392 used: CD45.1 APC (clone A20); CD45.2 BV786 (104); CD3 FITC (145-2C11); B220

393 FITC (RA3-6B2); TCRβ PE-Cy7 (H57-597); MHCII alexa700 (M5/114.15.2); Ly6G PE-

394 Cy7 (1A8); CD11b PB and APC (M1/70); CD11c PerCP/Cy5.5 (N418); F4/80 FITC and

395 alexa647 (BM8); CD44 FITC (IM7); CD62L PE (MEL-14); CD8α APC (53-6.7); CD4 PE

396 and PerCP/Cy5.5 (RM4-5); IFNγ FITC (XMG1.2); IL-10 PE (JES5-16E3). All antibodies

397 were from Biolegend. To measure intracellular cytokines in T cells following *ex vivo*

398 stimulation, cells were first stimulated in complete RPMI for 4 hours at 37°C with

399 500ng/ml PMA, 1µg/ml ionomycin and 10µg/ml brefeldin A (all Sigma). For myeloid cells,

400 cells were cultured as above either in the absence of exogenous stimulation (brefeldin

401 A alone) or with *E. coli* O55:B5 LPS (1µg/ml with brefeldin A; Sigma). To measure

402 antigen-specific cytokine production, CD4$^+$ cells were purified by magnetic separation

403 (Miltenyi Biotech) from the spleens of day 28 *L. donovani* infected CD45.2 WT and miR-

404 132$^{-/-}$ mice and cultured for 3 days with naïve splenocytes (CD45.1 WT mice) as a source

405 of antigen-presenting cells (0.5x10^6 CD45.2$^+$ *Ld* CD4$^+$, 1x10^6 CD45.1$^+$ naïve

406 splenocytes). Cells were cultured either alone or with 1.5x10^7 whole killed (freeze-

407 thawed) *L. donovani* amastigotes as a source of parasite antigen. Brefeldin A was added

408 as above for the final 4 hours of culture to permit accumulation of intracellular cytokines.

409 CD45.2 and CD45.1 staining was used to assess cytokine production by CD4 T cells

410 from L. donovani-infected and naïve mice, respectively. For all intracellular cytokine

411 staining, surface stained cells were fixed and permeabilised (20min at 4°C) using

412 Fixation/Permeabilisation solution before washes in Perm/Wash buffer (both BD

413 Biosciences). Cells were then staining with intracellular antibodies as above except in

414 Perm/Wash buffer. Appropriate isotype controls were included. For FACS analysis,

415 events were acquired on a LSRFortessa (BD Biosciences) before analysis with FlowJo

416 (FlowJo LLC). For cell sorting of splenic lymphocytes from naïve and *Ld*-infected

417   spleens, B cells were gated as B220$^+$ CD3$^-$; CD4 T cells as B220$^-$ CD3$^+$ CD4$^+$ CD8a$^-$;

418   and CD8 T cells as B220$^-$ CD3$^+$ CD4$^-$ CD8α$^+$. For purification of naïve and activated CD4

419   T cells from uninfected mice, single cell suspensions were prepared from pooled

420   spleens and peripheral LN (axillary, brachial and inguinal). CD4$^+$ cells were enriched

421   using CD4 microbeads and LS columns (both Miltenyi Biotec) before cell sorting of naïve

422   CD4 T cells (CD4$^+$ CD62L$^+$ CD44$^-$ CD11b$^-$ CD8a$^-$ MHCII$^-$). For cell sorting of splenic

423   myeloid cell populations, cells were gated as Fig. EV5C. Cell sorting was performed with

424   a MoFlo Astrios (Beckman Coulter) and sorted cells were typically >98% positive.

425

426   ***In vitro* activation of CD4 T cells**

427   Purified CD4 T cells were stimulated with 10μg/ml plate bound anti-CD3ε (clone 145-

428   2C11) and 2μg/ml soluble anti-CD28 (37.51) in RPMI 1640 as before in flat bottom 96

429   well plates. For Th1 polarisation, cells were also treated with 15ng/ml recombinant

430   mouse IL-12 and 5μg/ml anti-IL-4 (11B11), or for Th2 polarisation, 30ng/ml recombinant

431   mouse IL-4 and 5μg/ml anti-IFNγ (XMG1.2). Phenylephrine hydrochloride (Sigma) was

432   used at 10μM and added during both anti-CD3 dependent activation (4 days) and also

433   during rest in 10U/ml recombinant human IL-2 (2 days). All antibodies were from

434   Biolegend and were low endotoxin / azide free, and recombinant cytokines were from

435   Peprotech.

436

437   **MEF cell culture, siRNA and miRNA mimic treatment**

438   C57BL/6 MEFs were provided by Dr. D. Coverley (University of York, UK) and were

439   cultured in DMEM (high glucose and pyruvate; ThermoFisher) supplemented with 10%

440   FCS, pen-strep and L-glut as RPMI. For transfections, 5x10^4 cells per well were seeded

441   in 6 well plates and transfected the next day with ON-TARGETplus SMARTpool siRNA

442   (100nM), miRIDIAN miRNA mimics (50nM), or appropriate controls (all Dharmacon, GE

443   Healthcare) using TransIT-siQUEST transfection reagent (Mirus) and Opti-MEM

444   medium (ThermoFisher) for 6 hours before being replaced with complete DMEM. EL4

445   cells were grown in RPMI supplemented with 10% FCS and were transfected with

446   miRNA mimics using Neon Nucleofection as per manufacturer's instructions. Non-

447   targeting control (NTC) siRNAs or mimics were used as controls. Cells were harvested

448   48 hours after transfection.

449

450   **Quantitative reverse transcription PCR (qRTPCR)**

451   RNA was extracted from tissue samples or purified cell populations using QIAzol and

452   miRNeasy RNA extraction kits (QIAGEN) according to manufacturer's instructions.

453   Tissue samples were first dissociated in QIAzol using a Tissuelyser LT with stainless

454   steel beads (all QIAGEN, UK). For detection of mature miRNA, cDNA was synthesised

455   using Taqman miRNA reverse transcription kits, and levels determined with Taqman

456   miRNA assays and Taqman Universal PCR Master Mix (all ThermoFisher). For mRNA

457   transcripts, reverse transcriptions were carried out with Superscript III (ThermoFisher)

458   and random hexamer primers (Promega), and measured with Fast SYBR Green Master

459   Mix (ThermoFisher). PCR were performed using a StepOnePlus Real Time PCR

460   System (ThermoFisher) and relative transcript levels determined using the ΔΔCt method.

461   Mature miRNA levels were normalised to U6. RNA transcript levels in T cells from *L.*

462   *donovani*-infected mice and MEFs were normalised to HPRT. As *in vitro* CD4 T cell

463   activation changes HPRT, GAPDH and β-actin expression levels, U6 was also used to

464   normalise mRNA expression in day 0 and 1 naïve T cells. The following primer

465   sequences were used:

466   BTAF1: Forward: 5'GCCTTTGGAAAGCTTTTGTG3', Reverse:

467   5'CCAGTACCTGCCCCATGT3'. HPRT: Forward:

468   5'GCGTCGTGATTAGCGATGATGAAC3', Reverse:

469   5'ATCTCCTTCATGACATCTCGAGCAAGTC3'. POLR2F: Forward:

470   5'GAGGAGGACGAAGGACTTGA3', Reverse: 5'CCAGATGGGAGAATCTCGAC3'.

471   RPL12: Forward: 5'CGAAGATCGGTCCTCTGG3', Reverse:

472   5'AATTCTGAGACCCTTCCAGTCA3'. RPL18: Forward:

473 5'CGCATGATCCGAAAGATGA3', Reverse: 5'AACTTCCAGAATCCGCACAT3'.

474 RPL26: Forward: 5'AGAAGGCTAATGGCACAACC3', Reverse:

475 5'TCCAGCTTTAGCCTGGTGAT3'. RPL27: Forward:

476 5'TGAAAGGTTAGCGGAAGTGC3', Reverse: 5'CATGAACTTGCCCATCTCG3'.

477 RPL8: Forward: 5'CAACAGAGCCGTTGTTGGT3',   Reverse:

478 5'CAGCCTTTAAGATAGGCTTGTCA3'. RPS10: Forward:

479 5'GTGAGCGACCTGCAAGATTC3', Reverse: 5'CAGCCTCAGCTTTCTTGTCA3'.

480 RPS14: Forward: 5'AGTCTGGAGACGACGATCAGA3', Reverse:

481 5'CAGACACCAAACACATTCTCTCC3'. RPS30: Forward:

482 5'GGTCGCCCAGATCAAAGAT3', Reverse: 5'TGCCAGAAGCACGACTTG3'. RPS3A:

483 Forward: 5'TGGCAAGAAGGGAGCTAAGA3', Reverse:

484 5'GTGTCTTCCCGATGTTCCTAAT3'. RPS9: Forward:

485 5'ATCCGCCAACGTCACATTA3', Reverse: 5'TCTTCACTCGGCCTGGAC3'. RPSA:

486 Forward: 5'GGTCCATACGGCGTTGTT3', Reverse:

487 5'GCAGCAAGGAATTTGAGGAC3'. RPL14-ps1: Forward:

488 5'TGCTGCTGCTGCTAAAGCTA3', Reverse: 5'CAGCCTTCTTGCCTGGTC3'. RPL23-

489 ps3: Forward: 5'ATAAGGCCCGACGGAGAG3', Reverse:

490 5'GAATTAGCCATCTGGACTCAGTTT3'.

491

492 **SDS-PAGE, Western blotting, and protein synthesis assays**

493 Cells were washed twice in PBS and protein extracts prepared in RIPA buffer (150mM

494 NaCl, 10mM Tris pH 7.2, 5mM EDTA, 0.1% SDS, 0.1% Triton X-100, 1% sodium

495 deoxycholate, 1mM PMSF, 1% Protease Inhibitor cocktail P8340, 1% Phosphate

496 Inhibitors cocktails 2 and 3; all Sigma). Equal total amounts of protein were resolved on

497 SDS-PAGE gels and transferred to PVDF membranes (Millipore) using a BioRad SD

498 Semidry Transfer Cell, blocked for 2 hours at room temperature in 2% BSA

499 (ThermoFisher) or 5% milk powder (Sigma) in TBST (150mM NaCl, 7.7mM Tris HCl pH

500 8, 0.1% Tween 20; all Sigma) before overnight probing with primary antibodies at 4°C.

501 Antibodies were as follows: total CREB (clone 48H2), p-CREB S133 (87G3), BTAF1

502 (rabbit pAb #2637; all Cell Signaling Technology), p300 (clone NM11), Rpl27 (14980-1-

503 AP, Proteintech), Rps9 (14894-1- AP, Proteintech), β-actin (AC-15), GAPDH (9484; all

504 Abcam). Following extensive washing in TBST, blots were incubated with secondary

505 antibodies (goat anti-rabbit or mouse HRP; DAKO) for 1 hour at room temp, washed as

506 before, and developed with ECL Western Blotting Detection Reagent and Hyperfilm ECL

507 (both GE Healthcare). Densitometry was performed using Fiji / ImageJ.

508 Protein synthesis rates were measured by puromycin incorporation [31]. Cells were

509 pulsed for 10 mins with 10μg/ml puromycin (Sigma) and then washed and incubated for

510 an extra 50 mins before lysed and used for western blotting analysis. Puromycin was

511 detected with the monoclonal antibody clone 12D10 (Merck Millipore).

512

513 **RNA sequencing analysis**

514 Sequence reads were trimmed to remove adaptor sequences with Cutadapt and

515 mapped to mouse genome GRCm38 with HISAT2[49] including "rna-strandness FR"

516 option. Data available at GEO, accession number GSE125268. Transcriptome

517 assembly and quantification was performed using the Tuxedo pipeline (version

518 2.2.1)[50]. Cufflinks was used to assemble transcriptomes for each sample using the

519 GTF annotation file for the GRCm38 mouse genome. This was followed by running

520 Cuffmerge to merge individual sample transcriptomes into full transcriptomes.

521 Quantification and normalisation were carried out for each experiment using Cuffquant

522 and Cuffnorm. Differential expression on gene FPKM values was performed by

523 conducting paired and independent t-tests with Benjamini-Hochberg false discovery rate

524 correction. GSEA (http://software.broadinstitute.org/gsea) and STRING analysis

525 (http://string-db.org/) were performed where indicated. For analysis of genes

526 differentially expressed between WT and miR-132$^{-/-}$ CD4 T cells from *Ld*-infected

527 spleens, transcripts were required to be significantly dysregulated (>50% change from

528 WT levels, p<0.05) with FPKM values>1, and STRING settings were highest confidence

529 interactions only excluding text mining. Targetscan (http://www.targetscan.org/vert_71/)

530 was used to predict targets of miRNA from the miR-212/132 cluster (cumulative

531 weighted context score++ <-0.1).

532

533 **Luciferase assays**

534 BTAF1 3'UTR was amplified from mouse spleen cDNA (reverse transcribed with

535 Superscript II and oligo-dT primers; both ThermoFisher) using the following primers :

536 forward 5'<u>CTCGAG</u>TGCAACTGCTGCTAGCTCAGTTA3' (which introduces 5' Xho I

537 site) and reverse 5'<u>GCGGCCGC</u>TTATGAAAGCAGACAAGTA3' (which introduces 3'

538 Not I site). The 1.5 kb amplicon, which encompasses most of the 3' UTR of BTAF1

539 minus a 25nt 5' GC rich stretch, was cloned into pGEM-T vector (Promega) and

540 sequence verified. We also performed site directed mutagenesis to remove the miR-

541 212/132 seed sequence using QuikChange Site-Directed Mutagenesis (Agilent) with the

542 following primer pairs :

543 5'CTGAACCCTGTGGTAAAGACT**AAA**TACTGTAGCAGGGCCTGAAGC3'   and

544 5'GCTTCAGGCCCTGCTACAGTA**TTT**AGTCTTTACCACAGGGTTCAG3', resulting in

545 mutation of WT sequence (5'AACCCUGUGGUAAA<u>GACU**GUU**</u>U3') to mutant

546 (5'AACCCUGUGGUAAA<u>GACU**AAA**</u>U3'). Inserts were excised with XhoI and NotI

547 (NEB) and ligated into psiCHECK-2 (Promega). Luciferase assays were performed in

548 HeLa and 3T3 cells 24 hours after transfection as previously described[3].

549

550 **Statistical analysis**

551 Statistical analyses were carried out as indicated with Prism 5 (Graphpad Software Inc).

552 Two-way comparisons used paired or unpaired t-tests as indicated and multiple

553 comparisons used one-way ANOVA, followed by Bonferroni correction for multiple

554 testing. P values of <0.05 were considered significant. * p<0.05, ** p<0.01, *** p<0.001,

555 **** p<0.0001. Statistical significance in enrichment of RP genes (as in Fig. 2I) were

556 determined using Chi-Square test.

AUTHORS CONTRIBUTIONS

D.L. conceived, designed, and supervised the project. D.L. and J.P.H. designed experiments. P.M.K. and T.V.S. contributed to experimental design. J.P.H., K.M.S., N.B., P.G., S.A.H. and D.L. performed experiments. J.P.H., K.N., K.M.S., and D.L. analysed experiments. J.P.H. and D.L. wrote the manuscript. All authors critiqued and edited the manuscript.

CONFLICT OF INTERESTS

The authors declare no conflict of interest.

REFERENCES

1.   Mehta A, Baltimore D (2016) MicroRNAs as regulatory elements in immune system logic. *Nat Rev Immunol* **16**: 279-94

2.   Wanet A, Tacheny A, Arnould T, Renard P (2012) miR-212/132 expression and functions: within and beyond the neuronal compartment. *Nucleic Acids Res* **40**: 4742-53

583   3.   Lagos D, Pollara G, Henderson S, Gratrix F, Fabani M, Milne RS, Gotch F,

584   Boshoff C (2010) miR-132 regulates antiviral innate immunity through

585   suppression of the p300 transcriptional co-activator. *Nat Cell Biol* **12**: 513-9

586   4.   Nahid MA, Yao B, Dominguez-Gutierrez PR, Kesavalu L, Satoh M, Chan

587   EK (2013) Regulation of TLR2-mediated tolerance and cross-tolerance through

588   IRAK4 modulation by miR-132 and miR-212. *J Immunol* **190**: 1250-63

589   5.   Shaked I, Meerson A, Wolf Y, Avni R, Greenberg D, Gilboa-Geffen A, Soreq

590   H (2009) MicroRNA-132 potentiates cholinergic anti-inflammatory signaling by

591   targeting acetylcholinesterase. *Immunity* **31**: 965-73

592   6.   Taganov KD, Boldin MP, Chang KJ, Baltimore D (2006) NF-kappaB-

593   dependent induction of microRNA miR-146, an inhibitor targeted to signaling

594   proteins of innate immune responses. *Proc Natl Acad Sci U S A* **103**: 12481-6

595   7.   Mehta A, Mann M, Zhao JL, Marinov GK, Majumdar D, Garcia-Flores Y, Du

596   X, Erikci E, Chowdhury K, Baltimore D (2015) The microRNA-212/132 cluster

597   regulates B cell development by targeting Sox4. *J Exp Med* **212**: 1679-92

598   8.   Mehta A, Zhao JL, Sinha N, Marinov GK, Mann M, Kowalczyk MS, Galimidi

599   RP, Du X, Erikci E, Regev A*, et al.* (2015) The MicroRNA-132 and MicroRNA-

600   212 Cluster Regulates Hematopoietic Stem Cell Maintenance and Survival with

601   Age by Buffering FOXO3 Expression. *Immunity* **42**: 1021-32

602   9.   Hanieh H, Alzahrani A (2013) MicroRNA-132 suppresses autoimmune

603   encephalomyelitis by inducing cholinergic anti-inflammation: a new Ahr-based

604   exploration. *Eur J Immunol* **43**: 2771-82

605   10.   Iliopoulos D, Jaeger SA, Hirsch HA, Bulyk ML, Struhl K (2010) STAT3

606   activation of miR-21 and miR-181b-1 via PTEN and CYLD are part of the

607   epigenetic switch linking inflammation to cancer. *Mol Cell* **39**: 493-506

608 11.   Li D, Wang A, Liu X, Meisgen F, Grunler J, Botusan IR, Narayanan S, Erikci

609 E, Li X, Blomqvist L*, et al.* (2015) MicroRNA-132 enhances transition from

610 inflammation to proliferation during wound healing. *J Clin Invest* **125**: 3008-26

611 12.   Xiao J, Li Y, Prandovszky E, Karuppagounder SS, Talbot CC, Jr., Dawson

612 VL, Dawson TM, Yolken RH (2014) MicroRNA-132 dysregulation in Toxoplasma

613 gondii infection has implications for dopamine signaling pathway. *Neuroscience*

614 **268**: 128-38

615 13.   Ni B, Rajaram MV, Lafuse WP, Landes MB, Schlesinger LS (2014)

616 Mycobacterium   tuberculosis   decreases   human   macrophage   IFN-gamma

617 responsiveness through miR-132 and miR-26a. *J Immunol* **193**: 4537-47

618 14.   Magill ST, Cambronne XA, Luikart BW, Lioy DT, Leighton BH, Westbrook

619 GL, Mandel G, Goodman RH (2010) microRNA-132 regulates dendritic growth

620 and arborization of newborn neurons in the adult hippocampus. *Proc Natl Acad*

621 *Sci U S A* **107**: 20382-7

622 15.   Asmal M, Colgan J, Naef F, Yu B, Lee Y, Magnasco M, Luban J (2003)

623 Production of ribosome components in effector CD4+ T cells is accelerated by

624 TCR stimulation and coordinated by ERK-MAPK. *Immunity* **19**: 535-48

625 16.   Vo N, Klein ME, Varlamova O, Keller DM, Yamamoto T, Goodman RH,

626 Impey S (2005) A cAMP-response element binding protein-induced microRNA

627 regulates neuronal morphogenesis. *Proc Natl Acad Sci U S A* **102**: 16426-31

628 17.   Kaiser M, Wiggin GR, Lightfoot K, Arthur JS, Macdonald A (2007) MSK

629 regulate TCR-induced CREB phosphorylation but not immediate early gene

630 transcription. *Eur J Immunol* **37**: 2583-95

631 18.   Kaye P, Scott P (2011) Leishmaniasis: complexity at the host-pathogen

632 interface. *Nat Rev Microbiol* **9**: 604-15

633 19. Rodriguez A, Vigorito E, Clare S, Warren MV, Couttet P, Soond DR, van

634 Dongen S, Grocock RJ, Das PP, Miska EA*, et al.* (2007) Requirement of

635 bic/microRNA-155 for normal immune function. *Science* **316**: 608-11

636 20. Yang L, Boldin MP, Yu Y, Liu CS, Ea CK, Ramakrishnan P, Taganov KD,

637 Zhao JL, Baltimore D (2012) miR-146a controls the resolution of T cell responses

638 in mice. *J Exp Med* **209**: 1655-70

639 21. Grigoryev YA, Kurian SM, Hart T, Nakorchevsky AA, Chen C, Campbell D,

640 Head SR, Yates JR, 3rd, Salomon DR (2011) MicroRNA regulation of molecular

641 networks mapped by global microRNA, mRNA, and protein expression in

642 activated T lymphocytes. *J Immunol* **187**: 2233-43

643 22. Subramanian A, Tamayo P, Mootha VK, Mukherjee S, Ebert BL, Gillette

644 MA, Paulovich A, Pomeroy SL, Golub TR, Lander ES*, et al.* (2005) Gene set

645 enrichment analysis: a knowledge-based approach for interpreting genome-wide

646 expression profiles. *Proc Natl Acad Sci U S A* **102**: 15545-50

647 23. Szklarczyk D, Franceschini A, Wyder S, Forslund K, Heller D, Huerta-

648 Cepas J, Simonovic M, Roth A, Santos A, Tsafou KP*, et al.* (2015) STRING v10:

649 protein-protein interaction networks, integrated over the tree of life. *Nucleic Acids*

650 *Res* **43**: D447-52

651 24. Stubbington MJ, Mahata B, Svensson V, Deonarine A, Nissen JK, Betz AG,

652 Teichmann SA (2015) An atlas of mouse CD4(+) T cell transcriptomes. *Biol*

653 *Direct* **10**: 14

654 25. Tan TCJ, Knight J, Sbarrato T, Dudek K, Willis AE, Zamoyska R (2017)

655 Suboptimal T-cell receptor signaling compromises protein translation, ribosome

656 biogenesis, and proliferation of mouse CD8 T cells. *Proc Natl Acad Sci U S A*

657 **114**: E6117-E6126

658 26. Nosrati N, Kapoor NR, Kumar V (2014) Combinatorial action of transcription

659 factors orchestrates cell cycle-dependent expression of the ribosomal protein

660 genes and ribosome biogenesis. *FEBS J* **281**: 2339-52

661 27. Perry RP (2005) The architecture of mammalian ribosomal protein

662 promoters. *BMC Evol Biol* **5**: 15

663 28. Thomas MJ, Seto E (1999) Unlocking the mechanisms of transcription

664 factor YY1: are chromatin modifying enzymes the key? *Gene* **236**: 197-208

665 29. Auble DT, Wang D, Post KW, Hahn S (1997) Molecular analysis of the

666 SNF2/SWI2 protein family member MOT1, an ATP-driven enzyme that

667 dissociates TATA-binding protein from DNA. *Mol Cell Biol* **17**: 4842-51

668 30. Choukrallah MA, Kobi D, Martianov I, Pijnappel WW, Mischerikow N, Ye T,

669 Heck AJ, Timmers HT, Davidson I (2012) Interconversion between active and

670 inactive TATA-binding protein transcription complexes in the mouse genome.

671 *Nucleic Acids Res* **40**: 1446-59

672 31. Schmidt EK, Clavarino G, Ceppi M, Pierre P (2009) SUnSET, a

673 nonradioactive method to monitor protein synthesis. *Nat Methods* **6**: 275-7

674 32. Venters BJ, Irvin JD, Gramlich P, Pugh BF (2011) Genome-wide

675 transcriptional dependence on conserved regions of Mot1. *Mol Cell Biol* **31**:

676 2253-61

677 33. Alvarez-Saavedra M, Antoun G, Yanagiya A, Oliva-Hernandez R, Cornejo-

678 Palma D, Perez-Iratxeta C, Sonenberg N, Cheng HY (2011) miRNA-132

679 orchestrates chromatin remodeling and translational control of the circadian

680 clock. *Hum Mol Genet* **20**: 731-51

681 34. Ledda M, Di Croce M, Bedini B, Wannenes F, Corvaro M, Boyl PP,

682 Caldarola S, Loreni F, Amaldi F (2005) Effect of 3'UTR length on the translational

683 regulation of 5'-terminal oligopyrimidine mRNAs. *Gene* **344**: 213-20

684 35. Cope A, Le Friec G, Cardone J, Kemper C (2011) The Th1 life cycle:

685 molecular control of IFN-gamma to IL-10 switching. *Trends Immunol* **32**: 278-86

686 36. Zhang Z, Liu R, Townsend PA, Proud CG (2013) p90(RSK)s mediate the

687 activation of ribosomal RNA synthesis by the hypertrophic agonist phenylephrine

688 in adult cardiomyocytes. *J Mol Cell Cardiol* **59**: 139-47

689 37. Segev N, Gerst JE (2018) Specialized ribosomes and specific ribosomal

690 protein paralogs control translation of mitochondrial proteins. *J Cell Biol* **217**:

691 117-126

692 38. Xue S, Barna M (2012) Specialized ribosomes: a new frontier in gene

693 regulation and organismal biology. *Nat Rev Mol Cell Biol* **13**: 355-69

694 39. Anderson CF, Oukka M, Kuchroo VJ, Sacks D (2007)

695 CD4(+)CD25(-)Foxp3(-) Th1 cells are the source of IL-10-mediated immune

696 suppression in chronic cutaneous leishmaniasis. *J Exp Med* **204**: 285-97

697 40. Jankovic D, Kullberg MC, Feng CG, Goldszmid RS, Collazo CM, Wilson M,

698 Wynn TA, Kamanaka M, Flavell RA, Sher A (2007) Conventional T-

699 bet(+)Foxp3(-) Th1 cells are the major source of host-protective regulatory IL-10

700 during intracellular protozoan infection. *J Exp Med* **204**: 273-83

701 41. Nylen S, Maurya R, Eidsmo L, Manandhar KD, Sundar S, Sacks D (2007)

702 Splenic accumulation of IL-10 mRNA in T cells distinct from CD4+CD25+ (Foxp3)

703 regulatory T cells in human visceral leishmaniasis. *J Exp Med* **204**: 805-17

704 42. Owens BM, Beattie L, Moore JW, Brown N, Mann JL, Dalton JE, Maroof A,

705 Kaye PM (2012) IL-10-producing Th1 cells and disease progression are

706 regulated by distinct CD11c(+) cell populations during visceral leishmaniasis.

707 *PLoS Pathog* **8**: e1002827

708 43.   Saraiva M, Christensen JR, Veldhoen M, Murphy TL, Murphy KM, O'Garra

709 A (2009) Interleukin-10 production by Th1 cells requires interleukin-12-induced

710 STAT4 transcription factor and ERK MAP kinase activation by high antigen dose.

711 *Immunity* **31**: 209-19

712 44.   Gautam S, Kumar R, Maurya R, Nylen S, Ansari N, Rai M, Sundar S, Sacks

713 D (2011) IL-10 neutralization promotes parasite clearance in splenic aspirate

714 cells from patients with visceral leishmaniasis. *J Infect Dis* **204**: 1134-7

715 45.   Murphy ML, Wille U, Villegas EN, Hunter CA, Farrell JP (2001) IL-10

716 mediates susceptibility to Leishmania donovani infection. *Eur J Immunol* **31**:

717 2848-56

718 46.   Murray HW, Moreira AL, Lu CM, DeVecchio JL, Matsuhashi M, Ma X,

719 Heinzel FP (2003) Determinants of response to interleukin-10 receptor blockade

720 immunotherapy in experimental visceral leishmaniasis. *J Infect Dis* **188**: 458-64

721 47.   Ranatunga D, Hedrich CM, Wang F, McVicar DW, Nowak N, Joshi T,

722 Feigenbaum L, Grant LR, Stager S, Bream JH (2009) A human IL10 BAC

723 transgene reveals tissue-specific control of IL-10 expression and alters disease

724 outcome. *Proc Natl Acad Sci U S A* **106**: 17123-8

725 48.   Dalton JE, Maroof A, Owens BM, Narang P, Johnson K, Brown N,

726 Rosenquist L, Beattie L, Coles M, Kaye PM (2010) Inhibition of receptor tyrosine

727 kinases   restores   immunocompetence   and   improves   immune-dependent

728 chemotherapy against experimental leishmaniasis in mice. *J Clin Invest* **120**:

729 1204-16

730   49.   Kim D, Langmead B, Salzberg SL (2015) HISAT: a fast spliced aligner with

731   low memory requirements. *Nat Methods* **12**: 357-60

732   50. Trapnell C, Roberts A, Goff L, Pertea G, Kim D, Kelley DR, Pimentel H,

733   Salzberg SL, Rinn JL, Pachter L (2012) Differential gene and transcript

734   expression analysis of RNA-seq experiments with TopHat and Cufflinks. *Nat*

735   *Protoc* **7**: 562-78

736

737   **FIGURE LEGENDS**

738   **Figure 1: The miR-132/212 cluster regulates RP mRNA levels in CD4^{+} T cells from**

739   **chronically infected spleens.**

740   **A.** Expression of indicated miRNAs in sorted naïve (CD62L^{+} CD44^{-}) CD4^{+} T cells and

741   following *in vitro* stimulation with anti-CD3 / anti-CD28 (1-3 days), relative to levels in

742   cells prior to stimulation. Data from 3 independent experiments each using T cells pooled

743   from 4 WT mice. Significance determined by one-way ANOVA.

744   **B.** Expression of indicated miRNAs in purified spleen lymphocytes (B cells, CD4^{+} T cells

745   and CD8^{+} T cells) from d0 naive (white) and day 28 *L. donovani*-infected (grey) mice.

746   Expression of each miRNA normalized to levels in whole naïve spleen (dotted line). Data

747   is mean + SEM of 2 experiments with cells purified from 3-5 pooled spleens.

748   **C.** Volcano plot of RNAseq gene expression in splenic WT and *miR-132^{-/-}* CD4^{+} T cells

749   from d28 *L. donovani* infected mice. Fold change determined as log2 mean FPKM (*miR-*

750   *132[-/-]*/WT) from 4 WT and 5 *miR-132^{-/-}* mice. Transcripts significantly different between

751   WT and miR-132^{-/-} (p<0.05) are shown in red. Dotted box indicates transcripts

752   significantly up-regulated in miR-132^{-/-} CD4^{+} T cells by more than 50%.

753   **D.** STRING network analysis of significantly up-regulated transcripts in CD4^{+} T cells

754   from spleen of d28 *L. donovani* infected *miR-132^{-/-}* mice compared to WT cells. Cluster

755   of ribosomal proteins shown in green circle, with coding RP transcripts (black) and

756   pseudogenes (red) indicated. Secondary clusters are shown in grey.

E. Top enriched molecular function Gene Ontology terms for genes significantly up-regulated in CD4$^+$ T cells from spleens of infected *miR-132$^{-/-}$* mice compared to WT mice.

F. Volcano plot of all RP genes in splenic WT and *miR-132$^{-/-}$* CD4$^+$ T cells from d28 *L. donovani* infected mice. RPL genes are shown as circles, RPS genes as triangles, and pseudogenes as squares. Red symbols indicate significant difference between WT and miR-132$^{-/-}$ cells (p<0.05) whereas black non-significant.

G. Expression of RP transcripts determined by qPCR from *L. donovani* infected d28 WT (blue) and *miR-132$^{-/-}$* mice (red). N=9 for each WT and *miR-132$^{-/-}$* from 2 independent infection experiments. Box extends from 25-75th percentile, whiskers are minimum and maximum values, and horizontal lines indicate median. Significance determined by unpaired t-test.

H. Fold change of all RP transcripts (grey) in Th1 cells compared to naïve CD4$^+$ T cells. Data taken from RNA sequencing experiments described in reference 24. Fold changes in IL-10 (red) and IFNγ (blue) indicated for comparison. The statistical significance of the observed up-regulation of RP transcripts in Th1 cells is determined by Chi-squared test.

Data information: * p<0.05, ** p<0.01, *** p<0.001.

Figure 2: The B-TFIID cofactor BTAF1 is a direct miR-132 target in CD4$^+$ T cells.

A. Volcano plot (Log$_2$(Fold Change) vs -Log(P value)) of RNA gene expression in purified naïve CD62L$^+$ CD44$^-$ WT and *miR-132$^{-/-}$* CD4$^+$ T cells. Fold change determined as log2 mean FPKM (*miR-132$^{-/-}$*/WT) from 4 WT and 4 *miR-132$^{-/-}$* mice. Transcripts significantly different between WT and *miR-132$^{-/-}$* cells (p<0.05) shown in red.

B. Volcano plot of RNA gene expression in purified naïve CD62L$^+$ CD44$^-$ WT and *miR-132$^{-/-}$* CD4$^+$ T cells following 18hr *in vitro* stimulation with anti-CD3/anti-CD28 under Th1 conditions. Fold change determined as log2 mean FPKM (*miR-132$^{-/-}$*/WT) from 4 WT and 4 *miR-132$^{-/-}$* mice. Transcripts significantly different between WT and *miR-132$^{-/-}$* cells (p<0.05) shown in red.

785 **C.** Volcano plot of transcripts containing a conserved miR-212/132-3p target site in

786 naïve CD4$^+$ T cells from WT or *miR-132$^{-/-}$* mice.

787 **D.** Volcano plot of transcripts containing a conserved miR-212/132-3p target site in *in*

788 *vitro* polarised (Th1 condtions, 18h post stimulation) CD4$^+$ T cells from WT or *miR-132$^-$*

789 *$^{-}$* mice.

790 **E.** Volcano plot of transcripts containing a conserved miR-212/132-3p target site in

791 spleen CD4$^+$ T cells from d28 *L. donovani* infected WT or *miR-132$^{-/-}$* mice.

792 **F.** BTAF1 transcript levels determined by qRTPCR in WT (blue) or *miR-132$^{-/-}$* (red) in

793 naïve (d0) and Th1 polarised for 18h (d1) CD4$^+$ T cells, and CD4$^+$ T cells from d28 *L.*

794 *donovani* infected WT or *miR-132$^{-/-}$* mice. N=8-9 for each WT and *miR-132$^{-/-}$*.

795 **G.** Expression of BTAF1 protein in d0 naïve and d1 (18hr) Th1-polarised WT and *miR-*

796 *132$^{-/-}$* CD4$^+$ T cells, as determined by Western blot. Each lane from individual mouse,

797 and representative of two independent experiments.

798 **H.** Relative luciferase activity in HeLa transfected with plasmid containing WT *BTAF1*

799 3'UTR (white) or *BTAF1* 3'UTR on which the miR-132 binding site is mutated (grey)

800 downstream of renilla luciferase, in the presence of miR-132-3p or miR-212-3p mimics.

801 Error bars indicate SEM from eight replicate treatments.

802 Data information: Significance in (F) and (H) determined by unpaired t-test. * $p<0.05$, **

803 $p<0.01$.

804

805

806 **Figure 3: miR-132 and its targets p300 and BTAF1 control RP expression.**

807 **A.** mRNA levels of indicated RP transcripts determined by qRTPCR in MEFs transfected

808 with Non-targeting control (NTC) mimics (white) or miR-132-3p mimics (grey).

809 **B.** p300 and BTAF1 protein levels in MEF transfected with NTC mimics or miR-132-3p

810 mimics determined by Western blot. GAPDH was used as a loading control. Right panel

811 indicates mean + SEM of 4 experiments.

C. mRNA levels of indicated RP transcripts determined by qRTPCR in MEFs transfected with NTC siRNA (white) or p300 siRNA (grey).

D. mRNA levels of indicated RP transcripts determined by qRTPCR in MEFs transfected with NTC siRNA (white) or BTAF1 siRNA (grey).

E. mRNA levels of indicated RP transcripts determined by qRTPCR in MEFs transfected with NTC or miR-132-3p mimics and NTC siRNA or p300 or BTAF1 siRNAs for 48h. Levels are normalised to cells transfected with NTC siRNA and NTC mimic.

F. Puromycin incorporation (following 10-minute pulse and 50-minute chase) determined by western blot in MEFs transfected with NTC or miR-132-3p or miR-212-3p mimics.

Data information: Statistical significance is determined by unpaired t-test from 4-6 experiments. * $p<0.05$, ** $p<0.01$, *** $p<0.001$, **** $p<0.0001$.

Figure 4: miR-132 controls the balance between IL-10 and IFNγ production in CD4⁺ T cells.

A. Percentage of IFNγ⁺ live TCRβ⁺ CD4⁺ cells from *L. donovani* infected WT (blue) or *miR-132⁻ᐟ⁻* (red) mice, determined by intracellular cytokine staining. Data representative of 3 independent experiments with 3-5 mice per group.

B. Percentage of IFNγ⁺/IL-10⁺ live TCRβ⁺ CD4⁺ cells from *L. donovani* infected WT (blue) or *miR-132⁻ᐟ⁻* (red) mice, determined by intracellular cytokine staining. Data representative of 3 independent experiments with 3-5 mice per group.

C. IL-10 mRNA levels, determined by RNA-sequencing, in TCRβ⁺ CD4⁺ cells purified from spleens of *L. donovani* infected WT (blue) or *miR-132⁻ᐟ⁻* (red) mice (n=5 per group).

D. Percentage of IFNγ⁺ WT (blue) or *miR-132⁻ᐟ⁻* (red) *in vitro* polarised Th1 cells (6 days) in the presence or absence of phenylephrine (PE), determined by intracellular cytokine staining.

839 **E.** Percentage of IL10$^+$ WT (blue) or *miR-132$^{-/-}$* (red) *in vitro* polarised Th1 cells (6 days)

840 in the presence or absence of phenylephrine (PE), determined by intracellular cytokine

841 staining.

842 **F.** Total cell counts following *in vitro* Th1 polarisation (6 days) in the presence or absence

843 of phenylephrine (PE). For (D-E), cells were purified from 3 mice per group and 6

844 replicates performed.

845

846 Data information: For (A and B) statistical significance was determined by unpaired t-

847 test. For (D–F), significance was determined with 1-way ANOVA followed by

848 Bonferroni's multiple comparison test. * $p<0.05$, ** $p<0.01$, *** $p<0.001$. NS: not

849 significant.

850

851

852 **Figure 5: miR-132 promotes protective immunity to *L. donovani*.**

853 **A.** Liver LDU (Leishman Donovan units) at day 28 in infected WT mice treated with anti-

854 IL-10R antibody or isotype control antibody (left panel, n=5 mice per group), or at day

855 21 and day 28 from WT (blue), *IL-10$^{+/-}$* (open green circles) and *IL-10$^{-/-}$* (filled green

856 circles) mice (right panel n= 3-6 mice per group)

857 **B.** Day 28 splenic parasite burdens expressed as LDU with each data point representing

858 an individual mouse in WT (blue) and *miR-132$^{-/-}$* (miR-132-/-; red) mice. Data from 4

859 independent infection experiments.

860 **C.** Mean WT and *miR-132$^{-/-}$* spleen parasite burdens from the 4 independent

861 experiments shown in **(B)**. Lines link individual experiments.

862 **D.** Splenic parasite burdens relative to WT group (WT mean = 1) for each of the 4

863 experiments shown in (**B**), with each data point representing individual mouse.

864 **E.** Spleen size expressed as % body weight for d0 (naïve) or day 28 *L. donovani* infected

865 WT (blue) and *miR-132$^{-/-}$* (miR-132-/-; red) mice.

866 **F.** Liver size expressed as % body weight for d0 (naïve) or day 28 *L. donovani* infected
867 WT (blue) and *miR-132⁻/⁻* (red) mice.

868 Data information: Significance determined by unpaired t-test, and in (C) by paired t-test
869 of mean values. * p<0.05, ** p<0.01, *** p<0.001, **** p<0.0001.

870

871

872 **EXPANDED VIEW FIGURE LEGENDS**

873

874 **Expanded View Figure EV1: The miR-132/212 cluster regulates RP mRNA levels**
875 **in CD4⁺ T cells from chronically infected spleens.**

876 **A.** Expression of phosphorylated CREB (Ser133), total CREB and β-actin loading
877 control in naïve CD4⁺ T cells cultured for indicated number of hours in presence (+) or
878 absence (-) of anti-CD3 / anti-CD28, as determined by Western blot. Numbers indicate
879 intensity normalised to 1 hour unstimulated samples (lane 1) and corrected by β-actin
880 loading control. Representative of two independent experiments from 3 pooled mice
881 each.

882 **B.** Relative expression of miR-132-3p and miR-212-3p determined by qPCR in naïve
883 mouse CD4⁺ T cells stimulated with anti-CD3/anti-CD28 for 18 hours under Th0 (non-
884 polarising; white), Th1 (rIL-12/anti-IL-4; grey) or Th2 conditions (rIL-4/anti-IFNγ; black)
885 relative to level in naïve cells prior to stimulation.

886 **C.** Fold change of all RP transcripts (grey) in Th2 cells compared to naïve CD4 T cells.
887 Data taken from RNA sequencing experiments described in reference 24. Fold changes
888 in IL-10 (red) and IL-4 (blue) indicated for comparison. The statistical significance of the
889 observed up-regulation of RP transcripts in Th1 cells is determined by Chi-squared test.

890

891 **Expanded View Figure EV2: The B-TFIID cofactor BTAF1 is a direct miR-132 target**
892 **in CD4⁺ T cells.**

893   **A.** Volcano plot of RNAseq gene expression in purified CD62L$^+$ CD44$^-$ naïve WT cells

894   before and after 1 day (18h) stimulation with anti-CD3/anti-CD28. Fold change

895   determined as log2 mean FPKM (stimulated / pre-stimulation) from 4 WT mice.

896   Transcripts significantly different (p<0.05) shown in red.

897   **B.** Volcano plot of RNAseq gene expression in purified CD62L$^+$ CD44$^-$ naïve *miR-132$^{-/-}$*

898   cells before and after 1 day (18h) stimulation with anti-CD3/anti-CD28. Fold change

899   determined as log2 mean FPKM (stimulated / pre-stimulation) from 4 WT mice.

900   Transcripts significantly different (p<0.05) shown in red.

90C.   **C.** RNAseq gene expression levels of BTAF1 from pre-stimulation (d0), 18h anti-

902   CD3/anti-CD28 (d1) and the spleen of d28 *L. donovani* infection (Ld), from WT (blue)

903   and *miR-132$^{-/-}$* (red) mice (n=4-5 mice per group). Significance determined by unpaired

904   t-test as indicated.

905   **D.** Schematic of miR-212/132-3p 7mer-m8 site in the 3'UTR of *BTAF1* transcript,

906   showing conservation in human, mouse and chimp. The site is also conserved in, rhesus,

907   squirrel, rabbit, pig, cow, cat, dog, brown bat, elephant, opossum, macaw and chicken;

908   but not rat or lizard.

909   **E.** Relative luciferase activity in mouse 3T3 cells transfected with plasmid containing

910   WT (white) or miR-212/132-mutant (grey) *BTAF1* 3'UTR immediately downstream of

911   renilla luciferase, in the presence of miR-132-3p or miR-212-3p mimics. Error bars

912   indicate SEM from eight replicate treatments. Significance determined by unpaired t-

913   test.

914   **F.** Nucleotide sequences of mouse mature miRNA derived from miR-212/132 cluster.

915   Seed sequences indicated in bold.

916   **G.** Volcano plots of RNAseq gene expression for transcripts containing a poorly

917   conserved miR-132-5p site (upper panels) or a broadly evolutionary conserved miR-

918   212-5p site (lower panels). Fold change determined as log2 mean FPKM *miR-132$^{-/-}$*

919   /WT) from 4 WT and *miR-132$^{-/-}$* mice. Transcripts significantly different between WT and

920   miR-132$^{-/-}$ (p<0.05) shown in red. Data compares pre-stimulation naïve CD4 T cells (d0,

921 left panels); after 18h in vitro stimulation with anti-CD3/anti-CD28 (d1, middle panels);

922 and from the spleens of d28 *L. donovani*-infected mice. Transcripts that are significantly

923 different (p<0.05) and show >2 fold change in expression are indicated.

924 **H.** RNA levels of BACH2 (based on RNA-seq) from pre-stimulation (d0), 18h anti-

925 CD3/anti-CD28 (d1) and the spleen of d28 *L. donovani* infection (Ld), from WT (blue)

926 and *miR-132$^{-/-}$* (red) mice. Significance determined by unpaired t-test as indicated (n =

927 4-5 mice per group).

928 **I.** Log2 fold change (LFC) in RP genes after 18 hours *in vitro* stimulation of WT (blue)

929 or miR-132$^{-/-}$ naïve CD4$^+$ T cells with anti-CD3/anti-CD28. Percentages of up-regulated

930 and down-regulated transcirpts in WT (40%) and *miR-132$^{-/-}$* (61%) cells are shown.

931 Statistical significance is determined with Chi-squared test.

932 J) DeltaLFC (LFC$^{miR-132-/-}$ - LFC^{WT}) after 18 hours *in vitro* stimulation of WT (blue) or *miR-*

933 *132$^{-/-}$* naïve CD4$^+$ T cells with anti-CD3/anti-CD28. Significance is determined with Chi-

934 squared test. **Data information:** * p<0.05, ** p<0.01.

935

936

937 **Expanded View Figure EV3: miR-132 and its targets p300 and BTAF1 control RP**

938 **expression.**

939 **A.** mRNA levels of indicated RP transcripts determined by qRTPCR in MEFs transfected

940 with NTC mimics (white) or miR-212-3p mimics (grey). Cultures performed in triplicate.

941 Statistical significance determined by t-test.

942 **B.** Protein levels determined by western blot of RPL27 and RPS10 in MEFs transfected

943 with NTC, miR-132-3p, or miR-212-3p mimics for 48h.

944 **C.** Top enriched molecular function GO terms for miR-132/212-3p predicted target

945 genes. Predictions retrieved from Targetscan, total context score <-0.1.

946 **D.** Protein levels determined by western blot of BTAF1 and p300 in EL4 cells transfected

947 with NTC, miR-132-3p, or miR-212-3p mimics for 48h.

948 **Data information:** * p<0.05, ** p<0.01.

949

Expanded View Figure EV4: miR-132 controls the balance between IL-10 and IFNγ production in CD4$^+$ T cells.

A. Intracellular cytokine staining of WT or *miR-132$^{-/-}$* splenic live CD45.2$^+$ TCRβ$^+$ CD4$^+$ cells for IFNγ and IL-10 from d0 naïve and day 28 *L. donovani* infected mice following *ex vivo* stimulation (4hrs) with PMA and ionomycin.

B. Antigen-specific IFNγ and IL-10 production by splenic CD4$^+$ T cells from CD45.2$^+$ *L. donovani*-infected WT (blue) or *miR-132$^{-/-}$* (red) mice was assessed as described in materials and methods. Cells were cultured for 3 days in the absence of exogenous stimulation ("Neg", open circles) or with parasite antigen ("Ag", closed circles), after which cytokine production by CD4$^+$ T cells from infected ("CD45.2") or naïve mice ("CD45.1") was determined. Representative FACS plots for antigen-stimulated CD45.2$^+$ cells are shown. Significance determined by unpaired t-test, purified CD4$^+$ T cells from 4-5 mice per group.

963

Expanded View Figure 5: miR-132 promotes protective immunity to *L. donovani*.

A. Percentage of IL10$^+$ splenic live CD45.2$^+$ TCRβ$^+$ CD4$^+$ cells for IL-10 in d0 naïve and d21 in *L. donovani*-infected WT (blue), *IL-10$^{+/-}$* (open green) and *IL-10$^{-/-}$* (filled green) mice. d21 used due to accelerated parasite clearance and immune resolution in *IL-10$^{-/-}$* mice. Significance determined by ANOVA compared to WT group (n=3-5 per group).

B. Percentage of IFNγ$^+$ splenic live CD45.2$^+$ TCRβ$^+$ CD4$^+$ cells for IL-10 in d0 naïve and d21 in *L. donovani*-infected WT (blue), *IL-10$^{+/-}$* (open green) and *IL-10$^{-/-}$* (filled green) mice. d21 used due to accelerated parasite clearance and immune resolution in *IL-10$^{-/-}$* mice. Significance determined by ANOVA compared to WT group.

C. Gating strategy for defining distinct myeloid populations in infected mice shown in C. NBNT = non-B non-T i.e. B220$^-$ CD3$^-$ in d0 naïve and d28 infected WT mice.

D. Total spleen cell numbers or of indicated myeloid populations in d0 naïve and d28 *Ld*-infected WT (blue) or *miR-132$^{-/-}$* (red) mice. Myeloid cells gated as live CD45.2$^+$ CD3$^-$ B220$^-$ Ly6G$^-$ SS^{lo} singlets then; DC (CD11c$^+$ F4/80$^-$ MHCII$^+$); MφA (CD11b$^+$ F4/80$^+$ CD11c$^-$); MφB (CD11c$^+$ F4/80$^+$ CD11b^{lo}); and MφC (CD11c$^+$ F4/80$^+$ CD11b^{hi}). Bars show mean + SEM. Data pooled from two independent experiments (n=4-5 per group for each experiment). Significance determined by unpaired t-test as indicated.

E. Total spleen cell numbers or of indicated myeloid populations in d0 naïve and d21 *Ld*-infected WT (blue), *IL-10$^{+/-}$* (open green) and *IL-10$^{-/-}$* (filled green) mice (n=3-5 per group). Myeloid cells gated as in (**D**). Bars show SEM. Significance determined by one-way ANOVA and is shown compared to WT group.

F. Spontaneous and LPS-induced IL-10 production by indicated spleen myeloid populations (as in **D**) from N (naive) and *Ld*-infected mice (d28), determined by intracellular cytokine staining. n.d. not detected i.e. cell type absent in naïve mice. Significance determined by unpaired t-test as indicated, and data pooled from 2 independent experiments each with 3-5 mice per group. Bars show mean + SEM

G. Day 21 liver parasite burdens expressed as LDU (Leishman Donovan units) in WT (blue) and *miR-132$^{-/-}$* (red) mice. Each data point represents an individual mouse. Significance determined by unpaired t-test

H. Left hand panel: Day 28 liver parasite burdens expressed as LDU (Leishman Donovan units) in WT (blue) and *miR-132$^{-/-}$* (red) mice. Right hand panel shows same data expressed relative to WT levels (WT mean = 1). Data from 4 independent infection experiments with 4-5 mice per group per experiment. Significance determined by unpaired t-test.

I. Day 42 liver parasite burdens expressed as LDU (Leishman Donovan units) in WT (blue) and *miR-132$^{-/-}$* (red) mice. Each data point represents an individual mouse. Significance determined by unpaired t-test.

J. J.   Spleen size expressed as % body weight for naïve (= 0 parasite dose) or day 28 *L. donovani* infected WT (blue) and *miR-132$^{-/-}$* (red) mice. Mice were infected with 10,

1003   30 or 100x10^6 *L. donovani* amastigotes. Data pooled from 2 independent experiments

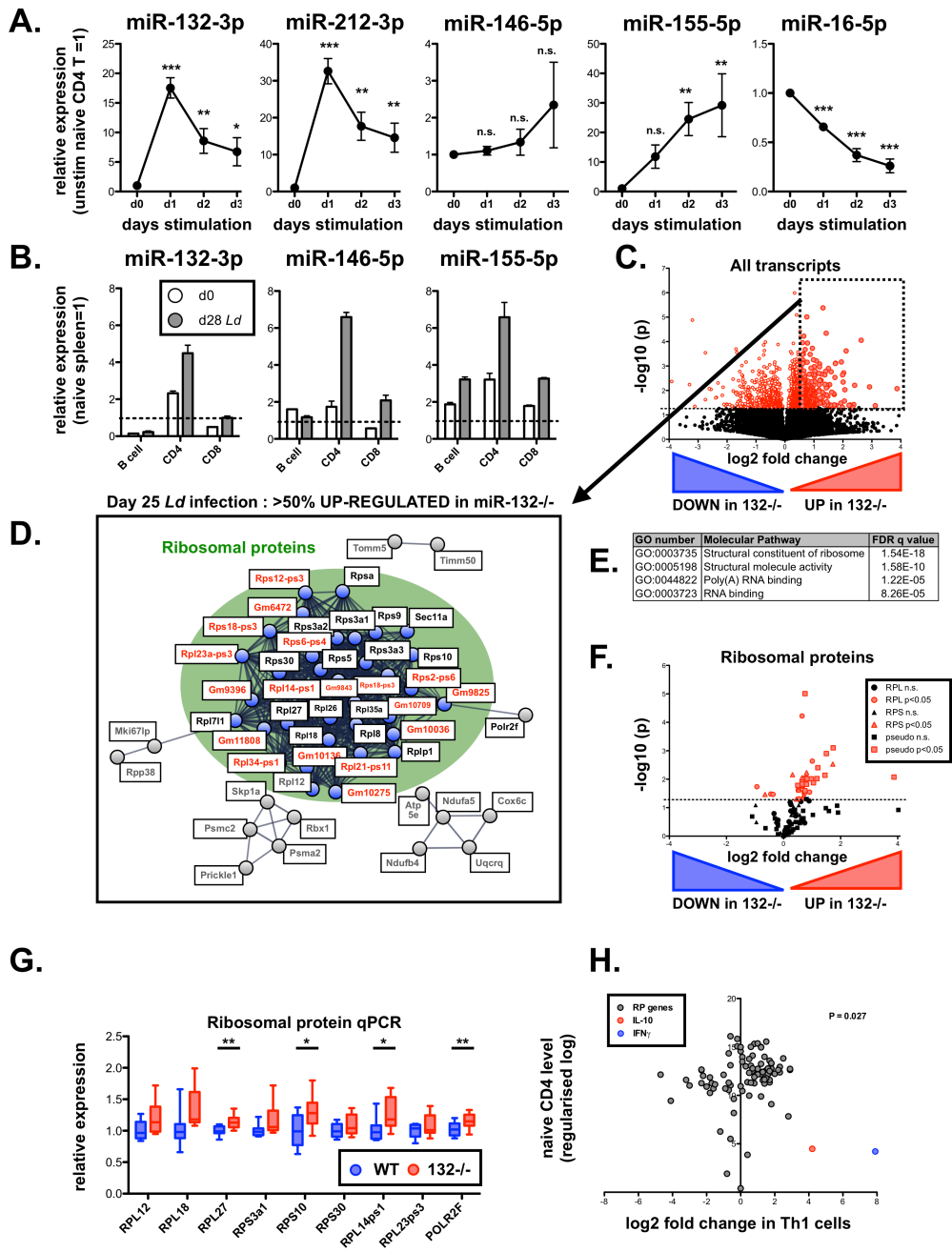1004   with 3-5 mice per group. Significance determined by unpaired t-test.

1005

1006   **K.** Liver size expressed as % body weight for naïve (= 0 parasite dose) or day 28 *L.*

1007   *donovani* infected WT (blue) and *miR-132$^{-/-}$* (red) mice. Mice were infected with 10, 30

1008   or 100x10^6 *L. donovani* amastigotes. Data pooled from 2 independent experiments with

1009   3-5 mice per group. Significance determined by unpaired t-test. Boxes for (J-K) extend

1010   from 25-75th percentile, whiskers are minimum and maximum values, and horizontal

1011   lines indicate median

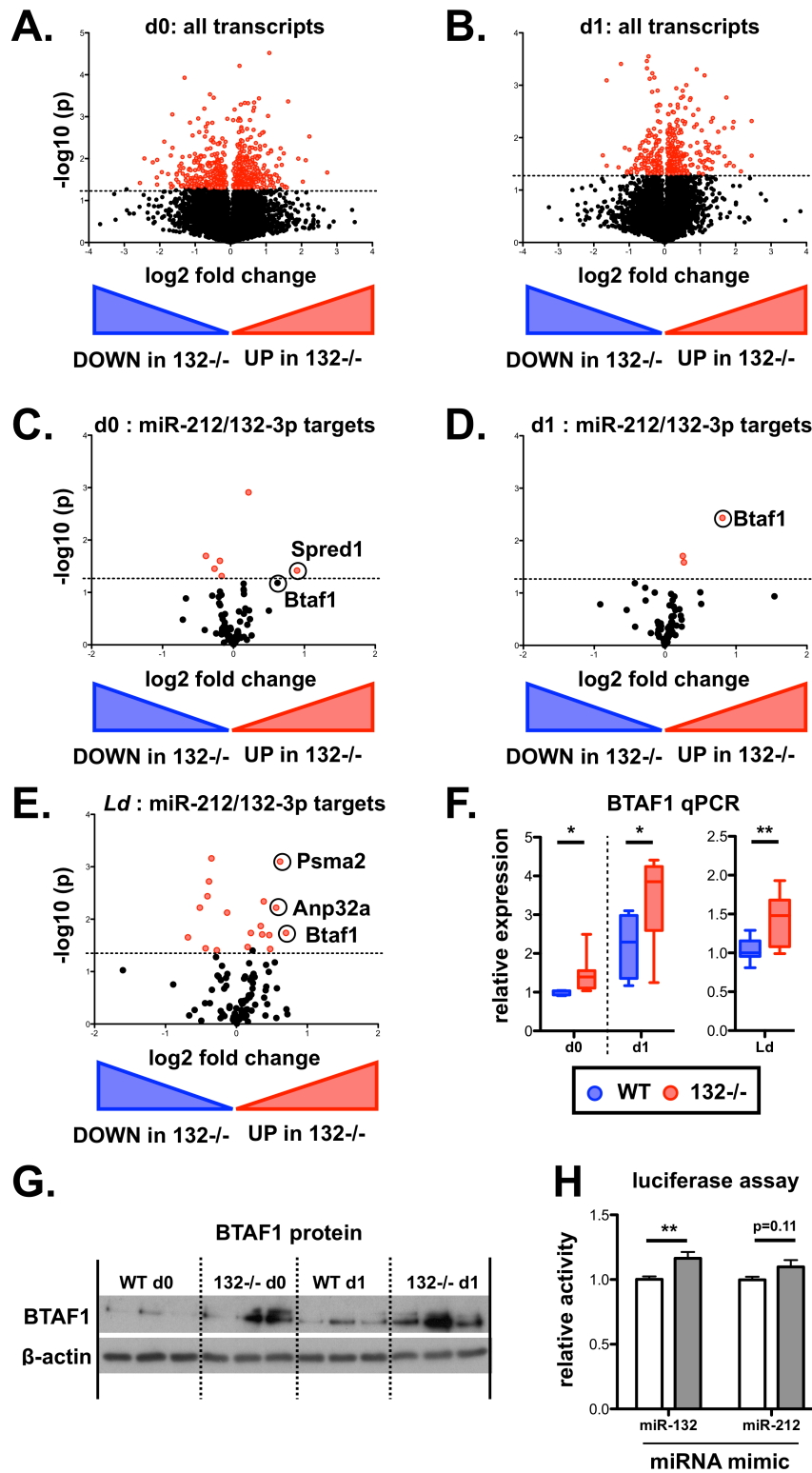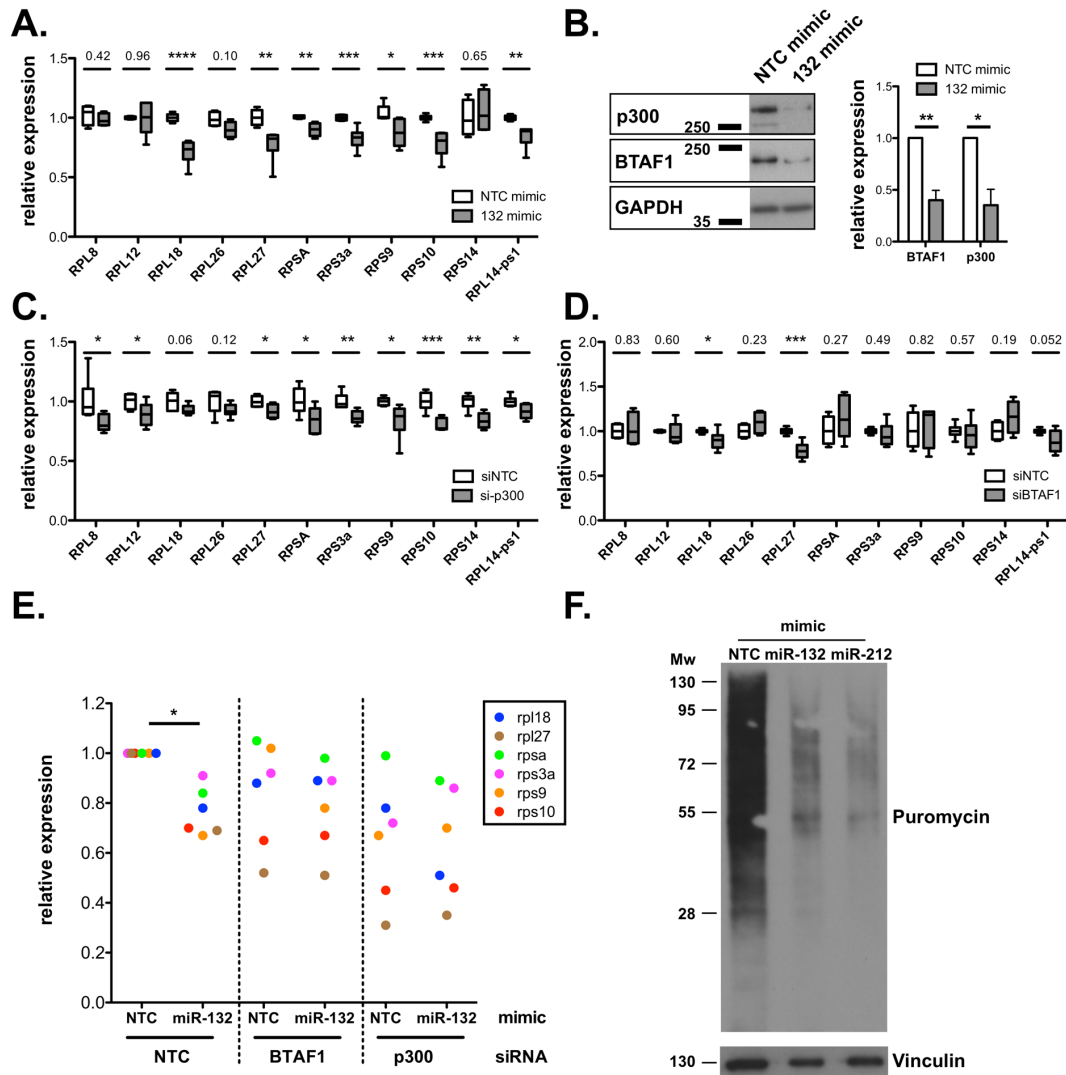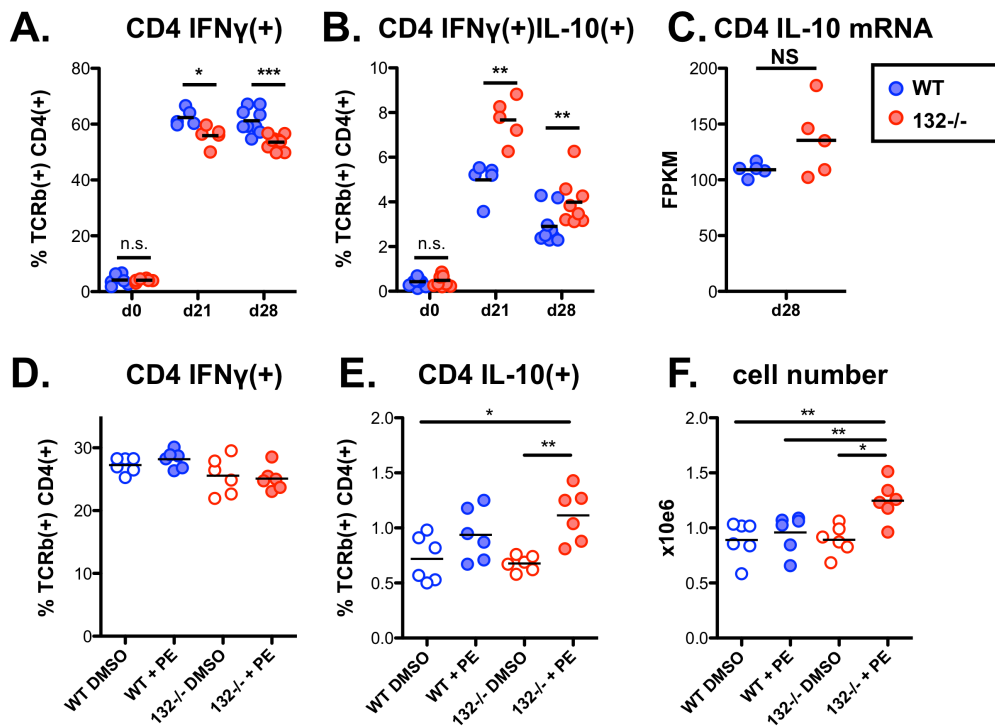1012   Data information: * $p<0.05$, ** $p<0.01$, *** $p<0.001$, **** $p<0.0001$.

1013

Fig. 1

A.

miR-132-3p | miR-212-3p | miR-146-5p | miR-155-5p | miR-16-5p

B.

miR-132-3p | miR-146-5p | miR-155-5p

C. All transcripts

DOWN in 132-/-   UP in 132-/-

D. Day 25 *Ld* infection : >50% UP-REGULATED in miR-132-/-

Ribosomal proteins

E.

GO number	Molecular Pathway	FDR q value
GO:0003735	Structural constituent of ribosome	1.54E-18
GO:0005198	Structural molecule activity	1.58E-10
GO:0044822	Poly(A) RNA binding	1.22E-05
GO:0003723	RNA binding	8.26E-05

F. Ribosomal proteins

DOWN in 132-/-   UP in 132-/-

G. Ribosomal protein qPCR

H.

P = 0.027

1014

Fig. 2

A. d0: all transcripts

B. d1: all transcripts

C. d0 : miR-212/132-3p targets

D. d1 : miR-212/132-3p targets

E. *Ld* : miR-212/132-3p targets

F. BTAF1 qPCR

G. BTAF1 protein

H. luciferase assay

1015

Fig. 3

A.

B.

C.

D.

E.

F.

1016

Fig. 4

A. CD4 IFNγ(+)

B. CD4 IFNγ(+)IL-10(+)

C. CD4 IL-10 mRNA

- ● WT
- ● 132-/-

D. CD4 IFNγ(+)

E. CD4 IL-10(+)

F. cell number

1017

Fig. 5

Fig. EV1

A.

B.

miR qPCR

C.

1019

Fig. EV2

A. WT : d0 Vs d1

B. miR-132-/- : d0 Vs d1

C. RNAseq BTAF1

D. miR-212/132 site in BTAF1 3'UTR

E. 3T3 luciferase assay

F.
```
mmu-mir-132-3p uaacagucuacagccauggucg
mmu-mir-212-3p uaacaguccuccagucacggcca
mmu-mir-132-5p aaccguggcuuucgauuguuac
mmu-mir-212-5p accuuggcucuagacugcuuacu
```

G.

DAY 0   DAY 1   *Ld*

miR-132-5p targets

miR-212-5p targets

H. BACH2 = 132-5p

I. p=0.01

J.

1020

45

Fig. EV3

A.

MEF + miR-212 mimic
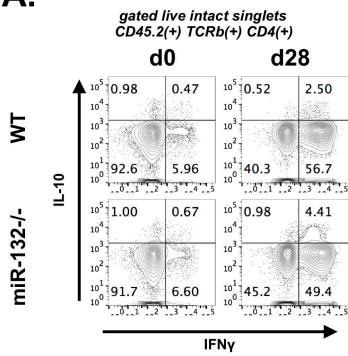

B.

C.

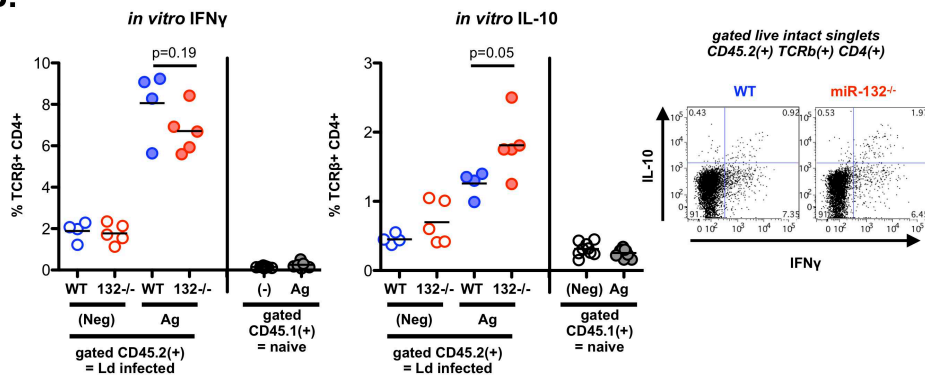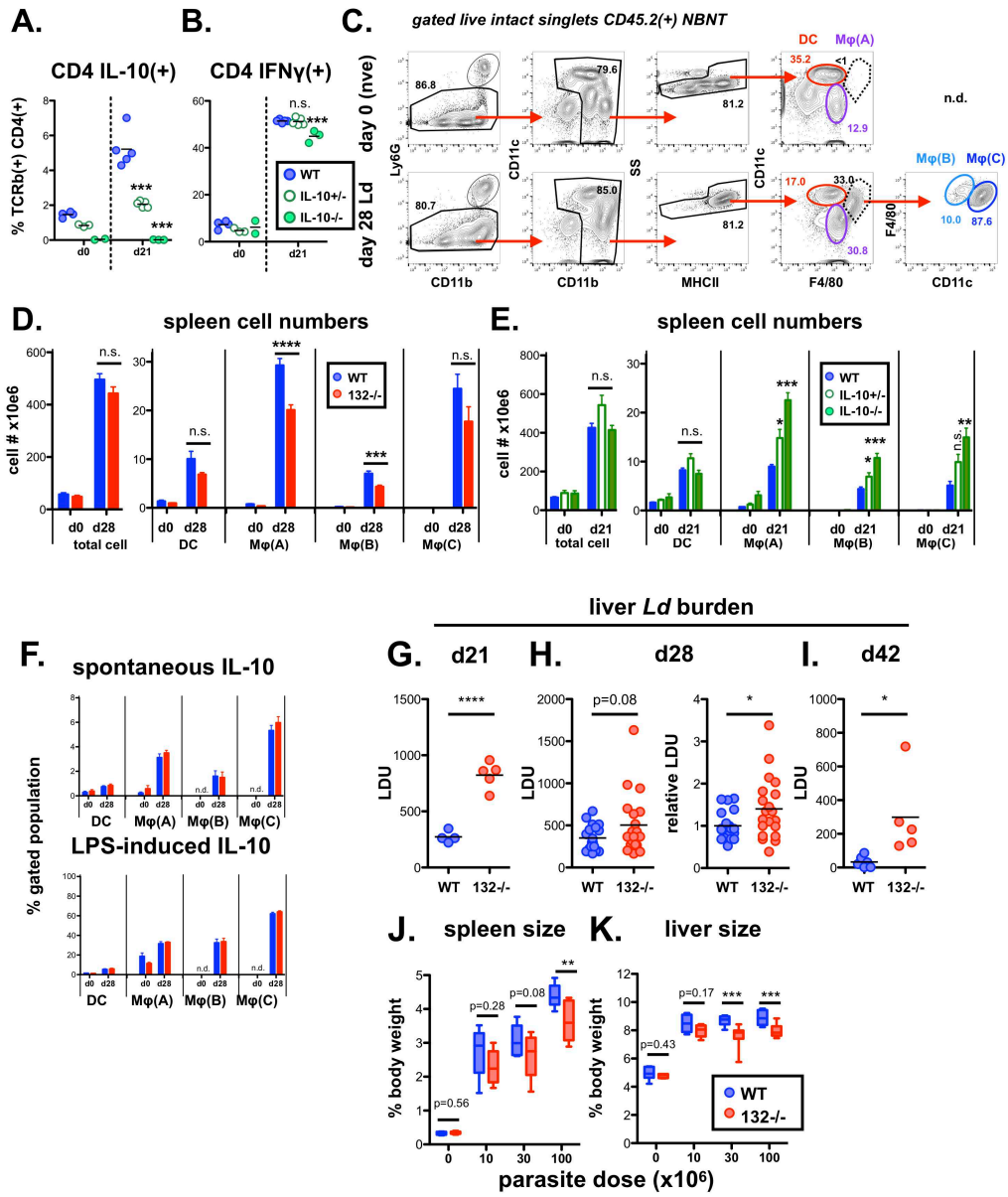| Molecular Pathway	FDR q-value
GO NUCLEIC ACID BINDING TRANSCRIPTION FACTOR ACTIVITY	3.83E-20
GO REGULATORY REGION NUCLEIC ACID BINDING	6.39E-16
GO SEQUENCE SPECIFIC DNA BINDING	2.55E-13
GO RNA POLYMERASE II TRANSCRIPTION FACTOR ACTIVITY SEQUENCE SPECIFIC DNA BINDING	4.55E-13
GO TRANSCRIPTION FACTOR ACTIVITY RNA POLYMERASE II CORE PROMOTER PROXIMAL REGION SEQUENCE SPECIFIC BINDING	2.99E-12
GO MACROMOLECULAR COMPLEX BINDING	4.98E-11
GO DOUBLE STRANDED DNA BINDING	1.41E-10
GO RNA BINDING	1.97E-10
GO CHROMATIN BINDING	1.97E-10
GO CORE PROMOTER PROXIMAL REGION DNA BINDING	1.69E-09

D.

1021

46

Fig. EV4

A.

gated live intact singlets
CD45.2(+) TCRb(+) CD4(+)

B.

in vitro IFNγ

in vitro IL-10

gated live intact singlets
CD45.2(+) TCRb(+) CD4(+)

Fig. EV5